

Vortex Dynamics for Two-Dimensional XY Models

Beom Jun Kim, Petter Minnhagen, and Peter Olsson

Department of Theoretical Physics, Umeå University, 901 87 Umeå, Sweden

Two-dimensional XY models with resistively-shunted junction (RSJ) dynamics and time-dependent Ginzburg-Landau (TDGL) dynamics are simulated and it is verified that the vortex response is well described by the Minnhagen phenomenology for both types of dynamics. Evidence is presented supporting that the dynamical critical exponent z in the low-temperature phase is given by the scaling prediction $z = 1/\tilde{\epsilon}T^{CG} - 2 \geq 2$ both for RSJ and TDGL and that the non-linear IV exponent a is given by $a = z + 1$ in the low-temperature phase. The results are discussed and compared with the results of other recent papers and the importance of the boundary conditions is emphasized.

PACS numbers: 74.50+r, 74.40+k, 74.25.Fy, 74.76.-w

I. INTRODUCTION

Superconducting films and two-dimensional (2D) Josephson junction arrays as well as ^4He films undergo Kosterlitz-Thouless (KT) type transitions from the superconducting/superfluid to the normal state.^{1,2} The KT transition is driven by thermally created vortex-antivortex pairs which start to unbind at the transition.² This means that some dominant characteristic features of the physics close to the transition are associated with vortex pair fluctuations. The great current interest in 2D vortex fluctuations stems from the fact that they are also present in high- T_c superconductors, not only in the case of thin films, but also in 3D samples just above the transition.³ It is therefore of interest to understand the properties associated with these thermally created vortices. Whereas there is a fairly good consensus on the static properties associated with vortex pair fluctuations,³ the dynamical aspects are less clear and some features are still controversial.

The knowledge of the dynamical properties of vortex fluctuations mainly comes from experiments on superconducting films and ^4He films,^{2,3} and from various model simulations.³ The theoretical attempts are so far on a rather phenomenological level^{2,4,5} with few exceptions.⁶ The more explicit knowledge derives from several kinds of simulations: XY models with time-dependent Ginzburg-Landau (TDGL) dynamics,⁷ XY models with resistively-shunted Josephson junction (RSJ) dynamics,^{8,9} the Coulomb gas model with Langevin dynamics,¹⁰ and the lattice Coulomb gas model with Monte Carlo dynamics.¹¹ There exist two phenomenological descriptions: the Ambegaokar-Halperin-Nelson-Siggia (AHNS) description⁴ and the Minnhagen phenomenology (MP)² (a more elaborate motivation for the MP version has also been attempted⁶). There are, likewise, two distinct proposals for the non-linear IV exponent a , i.e., a_{AHNS} ⁴ and a_{scale} ¹² with a corresponding proposal for a critical dynamical exponent $z = a_{scale} - 1$ ¹² in the low-temperature phase. It has also been argued that the non-linear IV exponent with the value a_{scale} applies to an intermedi-

ate current range whereas a_{AHNS} should be recovered in the true small-current limit.⁵ This argument rests on the assumption that for any finite current there are free vortices present and furthermore that these free vortices can be described by a conventional dynamics with $z = 2$.⁵

In this paper we present new extensive simulations of 2D XY models with RSJ as well as TDGL dynamics using a novel boundary condition. This enables us to obtain more information on the vortex dynamics for these models.

The situation is roughly the following: The MP form of the dynamical response gives a good description of the 2D XY models with TDGL dynamics,⁷ the Coulomb gas model with Langevin dynamics,¹⁰ and experiments on 2D superconductors.^{7,13,14} In the present paper we show that it also gives a good description of 2D XY models with RSJ dynamics. The dynamical exponent z for the lattice Coulomb gas with Monte Carlo dynamics has from simulations been inferred to have the scaling value $z = a_{scale} - 1$.¹¹ In the present paper we verify this result for the XY models with both RSJ and TDGL dynamics. This is seemingly in contradiction to the results in Ref. 8 that the 2D XY models with RSJ and TDGL dynamics behave differently and appear to have different z values. The non-linear IV exponent a has been found to have the scaling value a_{scale} for the Coulomb gas with Langevin dynamics¹⁰ and the lattice Coulomb gas with Monte Carlo dynamics.¹¹ However, contradictory results have been found for the XY model with RSJ dynamics, e.g., $a = a_{AHNS}$ in Ref. 9 and $a = a_{scale}$ in Ref. 12. In the present paper we find support for $a = a_{scale}$ for the 2D XY model with RSJ dynamics.

The picture emerging from our perspective is a generic vortex response well described by the MP form of the frequency response, the scaling exponent a_{scale} and the corresponding dynamical exponent $z = a_{scale} - 1$. According to our view this generic vortex response describes both Coulomb gas models and 2D XY models and is insensitive to the detailed type of the dynamics be it Coulomb gas Langevin-, Monte Carlo-, TDGL-, or RSJ-type.

The content of the present paper is the following: In Sec. II we describe the XY -type models and the relevant

correlation and response functions, as well as the relation to the vortex and Coulomb gas degrees of freedom. We also discuss the validity of linear response and the relation between the complex impedance and the dielectric function of the Coulomb gas. In the following section III the dynamical equations are described and the novel boundary condition is introduced and discussed. Sections IV and V contain our simulation results; Sec. IV the equilibrium ones and Sec. V the result when the system is driven by an external current. Finally in Sec. VI we summarize our results and make some final remarks.

II. XY MODEL

On a phenomenological level, a 2D superconductor/superfluid can be described by an order parameter $\psi(\mathbf{r}) = |\psi(\mathbf{r})|e^{i\theta(\mathbf{r})}$, where $|\psi(\mathbf{r})|^2$ is proportional to the superfluid density and $\nabla\theta(\mathbf{r})$ is proportional to the superfluid velocity.² The energy associated with the order parameter is the kinetic energy of the current and consequently the energy is proportional to $\int d^2r[\nabla\theta(\mathbf{r})]^2/2$.² A positive (negative) vortex centered at a certain point is associated with the topological excitation characterized by that the line integral $\int \nabla\theta(\mathbf{r}) \cdot d\mathbf{l}$ of an arbitrary small closed loop around the point is equal to 2π (-2π). There is a precise mapping between the vortices of a 2D superconductor and 2D Coulomb gas charges.² Since our interest in the present paper is the dynamical effects of the thermal vortex fluctuations, we will describe our results in the language of 2D Coulomb gas charges.

The *XY*-type models in a broad sense are models representing the continuum order parameter $\psi(\mathbf{r}) = |\psi(\mathbf{r})|e^{i\theta(\mathbf{r})}$ put on a lattice. Let us for convenience choose a square lattice. The discretized version is then $\psi_j = |\psi_j|e^{i\theta_j}$, where the index j denotes the lattice points. Let us simplify further by neglecting the variations of the magnitude of the order parameter and take $|\psi_j| = |\psi|$ to be a constant. The discretized version of the energy then takes the form

$$H_{XY} = J \sum_{\langle ij \rangle} U(\phi_{ij} = \theta_i - \theta_j), \quad (1)$$

where $J \propto |\psi|^2$ is termed the *XY* coupling constant and the sum is over nearest-neighbor pairs. The lattice constant is taken to be unity so that $\phi_{ij} = \theta_i - \theta_j$ corresponds to $\nabla\theta$ (in the direction from j to i). The function $U(\phi)$ has to be equal to $\phi^2/2$ for small ϕ in order to yield the correct continuum limit and in addition $U(\phi)$ has to be a periodic function of 2π since the phase angle θ_i for each lattice point is only defined upto a multiple of 2π . A possible choice for $U(\phi)$ is then

$$U(\phi) = 1 - \cos\phi$$

and with this choice the model is the usual 2D *XY* model or the planar rotor model. This particular interaction

would, e.g., arise if each lattice point was a small superconducting island which was Josephson coupled to its nearest neighbors, and the system is called a Josephson junction array (JJA). We will use this choice of the interaction in the present paper. However, from the point of view of vortex fluctuations any $U(\phi)$ fulfilling the necessary requirements stipulated above is a valid choice. A possible generalization is

$$U(\phi) = \frac{2}{p^2} \left[1 - \cos^{2p^2} \left(\frac{\phi}{2} \right) \right], \quad (2)$$

where $p = 1$ corresponds to the usual *XY* model. The practical point with such a generalization is that the vortex density increases with increasing p .¹⁵ Consequently the vortex response is sometimes easier to extract from simulations for a p -value larger than 1.⁷

The Boltzmann factor for a particular configuration is given by $e^{-H_{XY}/T}$ where T is the temperature in units of $k_B = 1$. From this all thermodynamic properties can be obtained.

The mapping between the *XY* model and the Coulomb gas representation is as follows:¹⁶ The effective temperature variable for the Coulomb gas charges is given by $T^{CG} = T/[2\pi J\langle U'' \rangle]$, where T is the temperature for the *XY* model, $\langle \dots \rangle$ denotes a thermal average, and $U'' = \partial^2 U / \partial \phi^2$. The supercurrent through a link is given by $JU' = J\partial U / \partial \phi$. The Coulomb gas charge n_l , corresponding to an elementary plaquette of the square lattice l , is given by the directed sum (corresponding to a line integral) over the four links $\langle ij \rangle$ making up the plaquette:¹⁶

$$n_l \equiv \frac{T^{CG}}{T} \sum_{\langle ij \rangle \in l} U'.$$

The charge density correlation function $g(r, t)$ can be obtained in the following way: If $\hat{G}(k, t)$ is defined as

$$\hat{G}(k, t) \equiv \left(\frac{T}{T^{CG}} \right)^2 \frac{\hat{g}(k, t)}{k^2} \quad (3)$$

then

$$\hat{G}(k, t) = \frac{1}{\Omega} \langle \hat{F}(k, t) \hat{F}(-k, t) \rangle,$$

where $\hat{F}(k, t)$ is the 1D Fourier transform

$$\hat{F}(k, t) = \sum_m F_m(t) e^{ikm},$$

m labels the rows of the lattice, and finally

$$F_m(t) = J \sum_{\langle ij \rangle \in m} U'[\phi_{ij}(t)],$$

where the summation is over all the links making up the row m . Linear response theory then links the charge

density correlation function $g(r, t)$ with the dielectric response function $1/\hat{\epsilon}(k, \omega)$ by⁷

$$\text{Re} \left[\frac{1}{\hat{\epsilon}(k, \omega)} \right] = \frac{1}{\hat{\epsilon}(k, 0)} + \frac{2\pi\omega T^{\text{CG}}}{T^2} \int_0^\infty dt \sin \omega t \hat{G}(k, t), \quad (4)$$

$$\text{Im} \left[\frac{1}{\hat{\epsilon}(k, \omega)} \right] = -\frac{2\pi\omega T^{\text{CG}}}{T^2} \int_0^\infty dt \cos \omega t \hat{G}(k, t), \quad (5)$$

where

$$\frac{1}{\hat{\epsilon}(k, 0)} = 1 - \frac{2\pi T^{\text{CG}}}{T^2} \hat{G}(k, 0). \quad (6)$$

The quantities $1/\hat{\epsilon}(0, \omega)$ and $\hat{G}(0, t)$ will be of particular interest in the present investigation.

The thermodynamic KT transition is characterized by

$$\lim_{k \rightarrow 0} \frac{1}{\hat{\epsilon}(k, 0)} = \frac{1}{\tilde{\epsilon}} > 0$$

below the transition and

$$\lim_{k \rightarrow 0} \frac{1}{\hat{\epsilon}(k, 0)} = 0$$

above. Precisely at the transition $\lim_{k \rightarrow 0} 1/\hat{\epsilon}(k, 0)T^{\text{CG}}$ jumps from the universal value $1/\tilde{\epsilon}T^{\text{CG}} = 4$ to zero.^{17,18} The equal time correlations fall off like power laws with distance below the transition and exponentially above.² For example, the correlation function $G(r, t = 0)$ falls off like

$$G(r, 0) \propto r^{-(1/\tilde{\epsilon}T^{\text{CG}} - 2)} \quad (7)$$

below the transition temperature. The fact that the correlations decay algebraically with distance reflects that the whole low-temperature phase is quasi-critical.

As explained in the previous section one motivation for the present paper is the question of the generality of the MP form for the dynamical response, which is given by²

$$\text{Re} \left[\frac{1}{\hat{\epsilon}(k = 0, \omega)} - \frac{1}{\hat{\epsilon}(0, 0)} \right] = \frac{1}{\tilde{\epsilon}} \frac{\omega}{\omega + \omega_0}, \quad (8)$$

$$\text{Im} \left[\frac{1}{\hat{\epsilon}(k = 0, \omega)} \right] = -\frac{2}{\tilde{\epsilon}\pi} \frac{\omega\omega_0 \ln \omega/\omega_0}{\omega^2 - \omega_0^2}. \quad (9)$$

The leading small ω behavior of Eqs. (8) and (9) reflects a $1/t$ decay for large t of the function $\hat{G}(k = 0, t)$.¹²

The two features $G(r, t = 0) \propto r^{-(1/\tilde{\epsilon}T^{\text{CG}} - 2)}$ and $\hat{G}(k = 0, t) = \int d^2r G(r, t) \propto 1/t$ can be turned into an argument for the dynamical critical index z in the following way:¹² We assume that $G(r, t)$ must be of the form

$$G(r, t) \propto \lambda^\alpha f(r/\lambda, t/\tau, a/r, \tau_a/t),$$

where λ is the correlation length or screening length which diverges in the low-temperature phase, τ is the corresponding diverging relaxation time so that

$$\tau \propto \lambda^z,$$

where z is the dynamical exponent. In addition we have a short distance scale a , i.e., the lattice constant or the size of a Coulomb gas particle and a non-diverging characteristic time scale τ_a , i.e., $\tau_a \propto l^2/D$ where D is a vortex or Coulomb particle diffusion constant and l is some non-diverging length scale like $l = a$ or $l = 1/\sqrt{n}$ where n is the density of Coulomb gas particles. Let us choose $t = 0$ and $r = \lambda$ so that

$$G(r, 0) \propto r^\alpha f(1, 0, a/r, \infty)$$

and make the *ad hoc* scaling assumption that

$$\lim_{r \rightarrow \infty} f(1, 0, a/r, \infty) = f(1, 0, 0, \infty) = \text{const.},$$

where $\text{const.} \neq 0$ and $\neq \pm\infty$. This requires $\alpha = -1/\tilde{\epsilon}T^{\text{CG}} + 2$ since $G(r, 0) \propto r^{-(1/\tilde{\epsilon}T^{\text{CG}} - 2)}$. We then also have that

$$\int d^2r G(r, t) = \lambda^{-\frac{1}{\tilde{\epsilon}T^{\text{CG}}} + 2} \int d^2r f(r/\lambda, t/\tau, a/r, \tau_a/t).$$

Now we choose $\lambda = t^{\frac{1}{z}}$ so that

$$\int d^2r G(r, t) = t^{(-\frac{1}{\tilde{\epsilon}T^{\text{CG}}} + 2)/z} \int d^2r f(r/t^{\frac{1}{z}}, 1, a/r, \tau_a/t)$$

and assume that

$$\lim_{t \rightarrow \infty} f(r/t^{\frac{1}{z}}, 1, a/r, \tau_a/t) = f(0, 1, a/r, 0) = \tilde{f}(a/r),$$

where $\tilde{f}(x)$ is a well-behaved function so that

$$\int d^2r G(r, t) \propto t^{(-\frac{1}{\tilde{\epsilon}T^{\text{CG}}} + 2)/z} \int d^2r \tilde{f}(a/r)$$

for large t . This is consistent with $\int d^2r G(r, t) \propto 1/t$ provided

$$z = \frac{1}{\tilde{\epsilon}T^{\text{CG}}} - 2. \quad (10)$$

The dynamical exponent z given by Eq. (10) has been inferred through simulations of the lattice Coulomb gas with Monte Carlo dynamics.¹¹ In the present paper we conclude that the same is true for the *XY* models both with RSJ and TDGL dynamics.

It has been argued by Dorsey,¹⁹ using scaling analysis, that for a 2D superconductor the exponent a in the non-linear *IV* characteristics $V \propto I^a$ has the value $a = z + 1$ precisely at the KT transition. It has further been suggested by Minnhagen¹² that since the whole

low-temperature phase is quasi-critical the same relation should apply throughout the low-temperature phase. This together with Eq. (10) leads to the prediction

$$a = a_{\text{scale}} = z + 1 = \frac{1}{\hat{\epsilon}T^{\text{CG}}} - 1. \quad (11)$$

The non-linear *IV* exponent $a = a_{\text{scale}}$ in Eq. (11) has been inferred through simulations for the Coulomb gas model with Langevin dynamics¹⁰ and the lattice Coulomb gas model with Monte Carlo dynamics.¹¹

The response to an imposed current is for a 2D superconductor given by the complex impedance $Z(\omega)^{2,20}$

$$\mathbf{E}(\omega) = Z(\omega)\mathbf{j}(\omega),$$

where $\mathbf{E}(\omega)$ is the frequency-dependent electric field and $\mathbf{j}(\omega)$ is the current density. Or equivalently for a quadratic sample $V(\omega) = Z(\omega)I(\omega)$, where V is the voltage across the superconductor in some direction and I is the total current in the same direction. The linear response function $Z^{-1}(\omega)$ is related to the Coulomb gas linear response function $1/\hat{\epsilon}(k=0, \omega)$ by

$$Z^{-1}(\omega) \propto \frac{\rho_0}{i\omega\hat{\epsilon}(k=0, \omega)}, \quad (12)$$

where ρ_0 is the density of superconducting electrons which for an *XY* model is given by $J\langle U'' \rangle$. This means that the effect on the vortex fluctuations of an imposed current is given by $1/\hat{\epsilon}(k=0, \omega)$. For small ω this is the dominant contribution.

It is instructive to consider the linear response to an imposed current directly in the the case of the *XY* model with RSJ dynamics. Let us consider a quadratic lattice and let $\langle ij \rangle_x$ be a link at position \mathbf{r} parallel to the x -axis and denote the difference in phase angle by $\phi_{ij} = \nabla_x \theta(\mathbf{r})$; when the coupling to the electromagnetic field is included ϕ_{ij} denotes the gauge invariant phase difference. The supercurrent through the link at time t is $JU'[\nabla_x \theta(\mathbf{r}, t)]$ and the normal current is proportional to $-\nabla_x \dot{\theta}(\mathbf{r}, t)$ where the dot denotes the time derivative. Thus the total current $i_x(\mathbf{r}, t)$ through the link is

$$i_x(\mathbf{r}, t) = -\nabla_x \dot{\theta}(\mathbf{r}, t) + JU'[\nabla_x \theta(\mathbf{r}, t)] \quad (13)$$

in some convenient unit system. The voltage in the RSJ model is proportional to the normal current so we can define the response function corresponding to the complex impedance as $Z(\mathbf{r} - \mathbf{r}', t - t') = P(\mathbf{r} - \mathbf{r}', t - t')$, where

$$P(\mathbf{r} - \mathbf{r}', t - t') = -\left. \frac{\partial \langle \nabla_x \theta(\mathbf{r}, t) \rangle}{\partial i_x(\mathbf{r}', t')} \right|_{i_x=0}. \quad (14)$$

It is shown in Appendix that the Fourier transform of P is given by

$$\hat{P}(\mathbf{k}, \omega) = \left[i\omega + \frac{\rho_0}{\hat{\epsilon}(\mathbf{k}, \omega)} \right]^{-1}, \quad (15)$$

where $\rho_0 = J\langle U'' \rangle$ so that

$$\hat{Z}(\mathbf{k}, \omega) = \left[1 + \frac{1}{i\omega} \frac{\rho_0}{\hat{\epsilon}(\mathbf{k}, \omega)} \right]^{-1}. \quad (16)$$

This means that the response to a uniform time varying current is given by $Z(\omega) = \hat{Z}(0, \omega)$. Below the KT transition we have

$$\lim_{\omega \rightarrow 0} \lim_{\mathbf{k} \rightarrow 0} \frac{1}{i\omega \hat{\epsilon}(\mathbf{k}, \omega)} = \infty$$

so that the static response to a uniform static current below the KT transition is non-linear. However, for any finite frequency the response is linear to the lowest order. One also notes that in the limit of high frequency $1/i\omega\hat{\epsilon}(\mathbf{k}, \omega)$ vanishes and \hat{Z} in Eq. (16) reduces to $Z(\infty) = 1$, which means that the response in this limit is given by the resistive shunt in the RSJ model. For smaller frequencies the response is given by the vortex fluctuation $Z(\omega) \propto i\omega\hat{\epsilon}(0, \omega)/\rho_0$ as already stated in Eq. (12).

III. DYNAMICAL EQUATIONS AND BOUNDARY CONDITIONS

Simulations by necessity involve lattices with a finite linear dimension L from which the results for the thermodynamic limit $L \rightarrow \infty$ have to be extracted. This means that in practice the choice of boundary condition is essential. The most commonly used boundary condition in order to extract the thermodynamic limit for the *XY* models is periodic boundary conditions (PBC) imposed on the phase angles θ_i . However, as discussed in Ref. 16, the PBC for the phase angles leads to a non-periodic boundary condition for the vortex interaction. The boundary condition for the phase angles which corresponds to a periodic vortex interaction is instead the fluctuating twist boundary condition (FTBC).¹⁶ The dynamics we are investigating in the present paper are linked to the vortex fluctuations and consequently the natural boundary condition is PBC for the vortices. This is the commonly used boundary condition for simulations of the lattice Coulomb gas with Monte Carlo dynamics¹¹ and the continuum Coulomb gas with Langevin dynamics.¹⁰ Thus the important point in the present context is that *PBC for the vortices* means *FTBC for the phase angles*. The FTBC for the phase angles has so far been used in connection with Monte Carlo simulations.¹⁶ In the present paper we extend the use of these boundary conditions to *XY* models with RSJ and TDGL dynamics. Of course the boundary condition should not matter in the limit $L \rightarrow \infty$. However, we in the present paper find that by using FTBC for the phase angles we are able to extract more information from our finite L simulations.

In this section, we briefly review the dynamical equations of motion for RSJ and TDGL in the case of PBC

for the phase angles. Then we construct the equations of motion for FTBC starting from total current conservation and the condition that the equations of motion should lead to the correct equilibrium distribution. We focus on the ordinary XY model, which corresponds to $p = 1$ case in the previous section, but the extension to a general p is straightforward.

We begin with an $L \times L$ array of the resistively-shunted junctions with PBC in both directions. In the RSJ dynamics of 2D XY model the net current from site i to site j is written as the sum of the supercurrent, the normal resistive current, and the thermal noise current:

$$i_{ij} = i_c \sin(\phi_{ij} = \theta_i - \theta_j) + \frac{V_{ij}}{r} + \Gamma_{ij},$$

where $i_c \equiv 2eJ/\hbar$ is the critical current of the single junction, V_{ij} is the potential difference across the junction, r is the shunt resistance, and the phase angles θ_i are periodic in both directions ($\theta_i = \theta_{i+L\hat{x}} = \theta_{i+L\hat{y}}$). The thermal noise current Γ_{ij} at temperature T is required to satisfy $\langle \Gamma_{ij}(t) \rangle = 0$ and $\langle \Gamma_{ij}(t) \Gamma_{kl}(0) \rangle = (2k_B T/r) \delta(t) (\delta_{ik} \delta_{jl} - \delta_{il} \delta_{jk})$. The current-conservation law at each site, together with the Josephson relation $d(\theta_i - \theta_j)/dt = 2eV_{ij}/\hbar$, allows us to write the equations of motion in the form:

$$\dot{\theta}_i = - \sum_j G_{ij} \sum'_k [\sin(\theta_j - \theta_k) + \eta_{jk}], \quad (17)$$

where the primed summation is over four nearest neighbors of j , G_{ij} is the lattice Green function on the square lattice with PBC, η_{jk} is the dimensionless thermal noise current defined by $\eta_{jk} \equiv \Gamma_{jk}/i_c$, and the unit of time is $\hbar/2e i_c$. The thermal noise current satisfies $\langle \eta_{ij}(t) \rangle = 0$ and

$$\langle \eta_{ij}(t) \eta_{kl}(0) \rangle = 2T(\delta_{ik} \delta_{jl} - \delta_{il} \delta_{jk}) \delta(t), \quad (18)$$

where T is in units of J/k_B .

In the TDGL dynamics with PBC, on the other hand, the equations of motion are given by²¹

$$\hbar \frac{d\theta_i(t)}{dt} = -\Gamma \frac{\partial H}{\partial \theta_i} + \Gamma_i(t),$$

where Γ is a dimensionless constant which determines the time scale of relaxation, $H \equiv -J \sum_{\langle ij \rangle} \cos(\theta_i - \theta_j)$ is the Hamiltonian of the usual XY model, and θ_i is periodic in both directions. The thermal noise term $\Gamma_i(t)$ is assumed to satisfy $\langle \Gamma_i(t) \rangle = 0$ and $\langle \Gamma_i(t) \Gamma_j(0) \rangle = 2\hbar\Gamma k_B T \delta_{ij} \delta(t)$. After rescaling the time and the temperature in units of $\hbar/\Gamma J$ and J/k_B , respectively, the equations of motion for TDGL dynamics are written as

$$\dot{\theta}_i = - \sum_j' \sin(\theta_i - \theta_j) + \eta_i, \quad (19)$$

where the thermal noise term $\eta_i \equiv \Gamma_i/\Gamma J$ satisfies $\langle \eta_i(t) \rangle = 0$ and

$$\langle \eta_i(t) \eta_j(0) \rangle = 2T \delta_{ij} \delta(t). \quad (20)$$

In numerical simulations for PBC, we use Eq. (17) and Eq. (19) for RSJ and TDGL dynamics, respectively, with the corresponding thermal noises satisfying Eqs. (18) and (20).

Next we consider the fluctuating twist boundary condition FTBC. In this case a variable $\Delta \equiv (\Delta_x, \Delta_y)$ is introduced and the phase difference ϕ_{ij} on the bond (i, j) is changed into¹⁶

$$\theta_i - \theta_j - \mathbf{r}_{ij} \cdot \Delta, \quad (21)$$

where $\mathbf{r}_{ij} \equiv \mathbf{r}_j - \mathbf{r}_i$ is a unit vector from site i to j , and the phase angles are periodic: $\theta_i = \theta_{i+L\hat{x}} = \theta_{i+L\hat{y}}$. In the study of equilibrium behaviors for FTBC using MC simulations, it is sufficient to know the Hamiltonian of the system¹⁶

$$H = -J \sum_{\langle ij \rangle} \cos(\theta_i - \theta_j - \mathbf{r}_{ij} \cdot \Delta). \quad (22)$$

In dynamical simulations, on the other hand, we must also have equations of motion for the new variables Δ_x and Δ_y in addition to the equations of motion for phase variables θ_i .

The physical situation we have in mind is a sample where no current passes through the boundary. For the RSJ model, which has local current conservation, this implies the total current conservation condition $\int d\mathbf{r}^2 \mathbf{i}(\mathbf{r}, t) = 0$, where $\mathbf{i}(\mathbf{r}, t) = [i_x(\mathbf{r}, t), i_y(\mathbf{r}, t)]$ is the total current density at point \mathbf{r} and the integral is over the whole sample. This condition can also be expressed as

$$\frac{V_x}{r} = -\frac{i_c}{L} \sum_{\langle ij \rangle_x} \sin(\theta_i - \theta_j - \Delta_x) - \eta_{\Delta_x} \quad (23)$$

(and the similar equation for the y -direction), where the summation $\sum_{\langle ij \rangle_x}$ is over all nearest-neighboring pairs in x -direction, V_x is the voltage drop over the sample, and η_{Δ_x} denotes the thermal noise current. This follows because the left hand side is recognized as the normal current whereas the right hand side is the negative of the sum of the supercurrent and the noise current. As discussed in connection with Eq. (13) the voltage is by the Josephson relation proportional to $\nabla \dot{\theta}(\mathbf{r}, t)$. For the voltage across the sample this means that [see Eq. (21)]

$$\dot{\Delta}_x = -\frac{2e}{\hbar L} V_x, \quad (24)$$

because the phase angles are by construction subject to periodic boundary conditions. Thus from Eqs. (23) and (24), we obtain the equations of motion for the twist variables:

$$\frac{d\Delta_x}{dt} = \frac{1}{L^2} \sum_{\langle ij \rangle_x} \sin(\theta_i - \theta_j - \Delta_x) + \eta_{\Delta_x}, \quad (25)$$

$$\frac{d\Delta_y}{dt} = \frac{1}{L^2} \sum_{\langle ij \rangle_y} \sin(\theta_i - \theta_j - \Delta_y) + \eta_{\Delta_y}, \quad (26)$$

where we have again written t in units of $\hbar/2eiri_c$. Next a noise correlation consistent with the equilibrium condition has to be found. To this end we make the ansatz of a standard white noise correlation $\langle \eta_{\Delta_x}(t)\eta_{\Delta_x}(0) \rangle = \langle \eta_{\Delta_y}(t)\eta_{\Delta_y}(0) \rangle = \sigma_{\Delta}^2 \delta(t)$ and determine the appropriate σ_{Δ}^2 in the following way: The equations of motion for the phase variables in FTBC are written as

$$\dot{\theta}_i = h_i - \sum_j \sum_k' G_{ij} \eta_{jk}, \quad (27)$$

with

$$h_i \equiv - \sum_j G_{ij} \sum_k' \sin(\theta_j - \theta_k - \Delta_{jk}) \quad (28)$$

and

$$\langle \eta_{ij}(t)\eta_{kl}(0) \rangle = \sigma^2 (\delta_{ik}\delta_{jl} - \delta_{il}\delta_{jk})\delta(t),$$

where $\sigma^2 = 2T$ [see Eq. (18)]. From the full equations of motion for RSJ model in FTBC [Eqs. (25) – (27)], we arrive at the Fokker-Planck equation:²²

$$\begin{aligned} \frac{\partial W}{\partial t} = & - \sum_i \frac{\partial}{\partial \theta_i} (h_i W) - \frac{\partial}{\partial \Delta_x} (h_x W) - \frac{\partial}{\partial \Delta_y} (h_y W) \\ & + \frac{1}{2} \sigma^2 \sum_{i,j} G_{ij} \frac{\partial^2 W}{\partial \theta_i \partial \theta_j} + \frac{1}{2} \sigma_{\Delta}^2 \left(\frac{\partial^2 W}{\partial \Delta_x^2} + \frac{\partial^2 W}{\partial \Delta_y^2} \right), \end{aligned}$$

where $W = W(\{\theta_i\}, \Delta_x, \Delta_y; t)$ is the probability distribution function and

$$h_x \equiv \frac{1}{L^2} \sum_{\langle ij \rangle_x} \sin(\theta_i - \theta_j - \Delta_x),$$

and the similar equation for h_y . The stationary solution, which satisfies $\partial W/\partial t = 0$, is of the correct form $W = e^{-\beta H}$ with the Hamiltonian given by Eq. (22) provided

$$\frac{\beta \sigma^2}{2} = \beta T = 1, \quad (29)$$

$$\frac{\beta \sigma_{\Delta}^2}{2} = \frac{1}{L^2}, \quad (30)$$

and consequently $\sigma_{\Delta}^2 = 2T/L^2$.

The equation of motion for the twist variables are hence of the Langevin form

$$\dot{\Delta} = -\Gamma_{\Delta} \frac{\partial H}{\partial \Delta} + \eta_{\Delta} \quad (31)$$

with $\Gamma_{\Delta} = 1/L^2$ and $\langle \eta_{\Delta_x}(t)\eta_{\Delta_x}(0) \rangle = \langle \eta_{\Delta_y}(t)\eta_{\Delta_y}(0) \rangle = (2T/L^2)\delta(t)$.

In the TDGL model the total current conservation condition can still be imposed whereas the local current conservation condition is relaxed. Thus Eqs. (25) and (26) remain unaltered whereas the equations for the phase angles are simplified to [compare Eqs. (19) and (21)]

$$\dot{\theta}_i = - \sum_j' \sin(\theta_i - \theta_j - \mathbf{r}_{ij} \cdot \Delta) + \eta_i, \quad (32)$$

where we have used the dimensionless time t by introducing the time unit of $\hbar/\Gamma J$ as in Eq. (19). Just as for the RSJ case one finds that $\Gamma_{\Delta} = 1/L^2$ and that the noise correlation $\langle \eta_{\Delta_x}(t)\eta_{\Delta_x}(0) \rangle = \langle \eta_{\Delta_y}(t)\eta_{\Delta_y}(0) \rangle = (2T/L^2)\delta(t)$ leads to the correct equilibrium. To some extent the TDGL dynamics may be viewed as a simplified version of the RSJ dynamics where the total current conservation is kept but the local current conservation is relaxed. Thus from this point of view it is perhaps not surprising that the two models (as we will see) have the same generic vortex dynamics.

The twist variable Δ plays an important role in our analysis of the vortex dynamics and there exists a rather direct connection between the twist and the vortices: The electric field $\mathbf{E}(t)$ due to the vortex current density \mathbf{j}_v is perpendicular and is, as a consequence of the Josephson relation, given by¹¹

$$E = \frac{h}{2e} \langle j_v(t) \rangle.$$

The connection between $\langle j_v(t) \rangle$ and $\dot{\Delta}$ is discussed in Ref. 16; when a vortex moves across the sample then the twist variable changes by $2\pi/L$. In other words, if the time t_0 is associated with the movement of a vortex across the sample, then we get $\dot{\Delta} = 2\pi/Lt_0 = 2\pi\langle \mathbf{v} \rangle/L^2$ where $|\langle \mathbf{v} \rangle| = L/t_0$ is the vortex velocity. If there are N_v moving vortices, then we obtain $\dot{\Delta} = 2\pi(N_v/L^2)\langle \mathbf{v} \rangle = 2\pi\langle \mathbf{j}_v \rangle$, which leads to the relation given by Eq. (24):

$$\dot{\Delta}_x = -\frac{2e}{\hbar L} V_x,$$

where V_x is the voltage drop across the sample in x -direction (we obtain the similar equation for Δ_y).

So far we have considered the situation when the total current in the sample is zero, which corresponds to no current passing over the boundary. Let us now consider the case when the total current is a constant dc current I_d in the x -direction. By following the steps from Eq. (23) to Eqs. (25) and (26) one obtains the modified equations of motion for the twist variable Δ

$$\frac{d\Delta_x}{dt} = \frac{1}{L^2} \sum_{\langle ij \rangle_x} \sin(\theta_i - \theta_j - \Delta_x) + \eta_{\Delta_x} - i_d \quad (33)$$

$$\frac{d\Delta_y}{dt} = \frac{1}{L^2} \sum_{\langle ij \rangle_y} \sin(\theta_i - \theta_j - \Delta_y) + \eta_{\Delta_y} \quad (34)$$

with $i_d = I_d/L$ in units of i_c . The voltage drop in the x -direction [see Eq. (24)] is given by

$$V_x = -L\dot{\Delta}_x \quad (35)$$

with V_x in units of ri_c for RSJ and in units of $\Gamma J/2e$ for TDGL, respectively. Thus the equations of motion in the presence of an externally imposed dc current I_d in the x -direction are given by Eqs. (27), (33), and (34) for RSJ and by Eqs. (32), (33), and (34) for TDGL.

An alternative and commonly used method in numerical simulations of the current-driven XY model is to impose uniform currents through the boundary in one direction. This requires an open boundary condition for the phase angles in the direction of the applied current and the periodic boundary condition can only be kept in the perpendicular direction.²³ This means that an open boundary is explicitly introduced. One advantage with the present method is that the periodic boundary conditions on the phase angles are kept and no explicit boundary is introduced.

In the following two sections we present the results obtained from the dynamical equations described in the present section both for the PBC and the FTBC.

IV. SIMULATION RESULTS

In this section, we present simulation results for the TDGL and RSJ dynamics with periodic boundary conditions PBC and the fluctuating twist boundary conditions FTBC. For PBC, we use Eqs. (17) and (18) in the RSJ case and in the TDGL case Eqs. (19) and (20). For FTBC, we use Eqs. (25) – (27) for RSJ, and Eqs. (25), (26), and (32) for TDGL.

We integrate the equations of motion by discretizing time into small steps Δt . At each step the appropriate random noise, generated from a uniform distribution, is introduced with $\langle \eta_{ij}(t)^2 \rangle = 2T/\Delta t$ for RSJ and $\langle \eta_i(t)^2 \rangle = 2T/\Delta t$ for TDGL [see Eqs. (18) and (20)]. We want to integrate to as long times as possible. On the other hand the larger Δt we choose the larger is the error introduced by the discretization. In order to get a handle of the choice for Δt we use the following identity: Let us introduce a local variable a_k on one particular site k . The Hamiltonian of the system is then

$$H = \sum_{\langle ij \rangle} U(\theta_i - \theta_j + a_i - a_j)$$

with $a_i \neq 0$ for $i = k$ and $a_i = 0$ otherwise, and the partition function is given by

$$Z = \int \prod_i d\theta_i \exp(-\beta H)$$

with the inverse temperature $\beta \equiv 1/T$. After a simple change of variable $\theta_i + a_i \rightarrow \theta_i$, we find that Z does in fact not depend on a_k and thus

$$\frac{\partial^2 \ln Z}{\partial a_k^2} = 0,$$

from which we conclude that

$$4\langle U'' \rangle = \frac{1}{T} \left\langle \left[\sum_j' U'(\theta_k - \theta_j) \right]^2 \right\rangle,$$

and thus

$$T = \tilde{T} \quad (36)$$

provided we have defined \tilde{T} by the local correlations

$$\tilde{T} \equiv \frac{\left\langle \left[\sum_j' U'(\theta_k - \theta_j) \right]^2 \right\rangle}{4\langle U'' \rangle}, \quad (37)$$

where the summation is over four nearest neighbors (denoted by j) of site k . The point is now that for a finite Δt one finds that $\tilde{T} > T$. This is illustrated in Fig. 1 where \tilde{T} is plotted as a function of the time step Δt for a fixed T . In the present simulations we use the time step $\Delta t = 0.01$ for TDGL and $\Delta t = 0.05$ for RSJ. These choices make \tilde{T} differ from T by less than 3%.

The fact that $\tilde{T} > T$ for a finite time step suggests that the effect of the finite time step to some extent is equivalent to an increased temperature. We have tried to take this into account when analyzing quantities related to $1/\epsilon$ by noting that for FTBC one has $1/\hat{\epsilon}(0, 0) = 0$,¹⁶ which means that [compare Eq. (6)]

$$T = \frac{\hat{G}(0, 0)}{\langle U'' \rangle}.$$

Thus we can estimate an effective temperature by $T^{\text{eff}} = \hat{G}(0, 0)/\langle U'' \rangle$. For example, for $T = 0.80$ and the time step $\Delta t = 0.05$ we for RSJ get $T^{\text{eff}} \approx 0.82$ whereas we for TDGL and the time step $\Delta t = 0.01$ get $T^{\text{eff}} \approx 0.803$.

A. Dynamical Response Functions with Periodic Boundary Conditions

We will first consider the vortex dynamics as reflected in the complex dielectric function given by Eqs. (4) and (5). It has so far been established that the MP form Eqs. (8) and (9) gives a good representation of the experimental data,¹³ as well as the simulation data for the TDGL dynamics of the XY model on a square lattice with $p = 2$ and on the triangular lattice with $p = 1$,⁷ and the 2D Coulomb gas model.¹⁰ In the present investigation we find that the same is true for the XY model with RSJ dynamics. This is illustrated in Fig. 2 which shows the real and imaginary parts of $1/\hat{\epsilon}(k = 0, \omega) - 1/\hat{\epsilon}(0, 0)$

with RSJ dynamics for $T = 0.85$. The full line in the figure has been obtained from a least-square fit to the MP form of the real part in Eq. (8) with two free parameters ($\tilde{\epsilon}$ and ω_0), and the broken line has been obtained by using the same values of the parameters in Eq. (9). The MP form has the characteristic feature that the ratio is $|\text{Im}[1/\tilde{\epsilon}(0, \omega)]|/\text{Re}[1/\tilde{\epsilon}(0, \omega) - 1/\tilde{\epsilon}(0, 0)] = 2/\pi$ at the frequency where the imaginary part has its maximum. One sees directly in Fig. 2 (i.e., without any curve fitting) that the dotted vertical line is close to this maximum and it is hence easy to verify that the ratio is indeed close to $2/\pi$. In short our present simulations of the complex dielectric function confirm that the RSJ dynamics is well described by the MP form at temperatures below as well as somewhat above the critical temperature in agreement with what was found earlier for the TDGL dynamics in Ref. 7.

As pointed out in connection with Eqs. (8) and (9), the leading small ω -dependence of the MP form

$$\text{Re} \left[\frac{1}{\tilde{\epsilon}(0, \omega)} - \frac{1}{\tilde{\epsilon}(0, 0)} \right] \propto \omega$$

and

$$\text{Im} \left[\frac{1}{\tilde{\epsilon}(0, \omega)} \right] \propto \omega \ln \omega$$

reflects that $\hat{G}(\mathbf{k} = 0, t) \propto 1/t$ for large t . More precisely,

$$\hat{G}(0, t) = \frac{T^2}{\pi^2 T^{\text{CG}}} \int_0^\infty \frac{\sin \omega t}{\omega} \text{Re} \left[\frac{1}{\tilde{\epsilon}(0, \omega)} - \frac{1}{\tilde{\epsilon}(0, 0)} \right] d\omega,$$

we find for the MP form

$$\hat{G}^{\text{MP}}(0, t) = \frac{T^2}{\pi^2 \tilde{\epsilon} T^{\text{CG}}} [\text{Ci}(\omega_0 t) \sin \omega_0 t - \text{si}(\omega_0 t) \cos \omega_0 t], \quad (38)$$

where the cosine and the sine integrals are defined by $\text{Ci}(x) \equiv - \int_x^\infty dt \cos t/t$ and $\text{si}(x) \equiv - \int_x^\infty dt \sin t/t$, respectively. In the limit of $\omega_0 t \rightarrow \infty$, Eq. (38) reduces to

$$\hat{G}^{\text{MP}} \approx \frac{T^2}{\pi^2 \tilde{\epsilon} T^{\text{CG}}} \frac{1}{\omega_0 t}.$$

This $1/t$ tail in the vortex correlations has been verified in Ref. 12 for TDGL dynamics and in Ref. 10 for the Coulomb gas model. We will here verify the same result for the RSJ dynamics.

The, by necessity, finite lattice sizes used in the simulations introduce a finite relaxation time τ_G at large t for the zero- k mode. By studying the lattice size dependence of $\hat{G}(0, t)$ we have found that this finite size induced relaxation changes the large- t decay from $1/t$ to $\frac{1}{t} \exp(-t/\tau_G)$. In fact we have found that $\hat{G}(0, t)$ for finite lattices to a good approximation is of a modified-MP form (MMP):

$$\hat{G}^{\text{MMP}} \equiv \hat{G}^{\text{MP}} \exp(-t/\tau_G). \quad (39)$$

Figure 3 shows $\ln[t\hat{G}(0, t)]$ as a function of time for the system sizes $L = 6, 8, 10, 12, 16$, and 64 in case of (a) RSJ and (b) TDGL dynamics at $T = 0.85$. The full drawn curves are least-square fits to Eq. (39). As is apparent from Fig. 3, $t\hat{G}$ approaches a constant for large lattice sizes verifying that \hat{G} indeed goes as $1/t$ for large t both for RSJ and TDGL dynamics.

The fits to the MMP form (full drawn curves in Fig. 3) show that $\ln t\hat{G}(0, t)$ goes as $-t/\tau_G$ for large t . In Fig. 4 we have plotted τ_G [determined by the fit to Eq. (39)] as a function of lattice size L in a lin-log plot. From finite-size scaling we expect that in the low-temperature phase τ_G diverges as $\tau_G \propto L^z$ for large L where z is the dynamical critical exponent. This behavior corresponds to straight lines in Fig. 4 and the full straight lines in the figure suggest that the asymptotic scaling is reached already for relatively small L . Assuming that this is the case, we find from the slopes of the lines that for $T = 0.85$ $z \approx 1.6$ in case of RSJ and $z \approx 2$ for TDGL. Thus the z values in case of PBC are *different* for the RSJ and the TDGL dynamics. This difference between RSJ and TDGL in case of periodic boundary conditions was also found by Tiesinga *et al.* in Ref. 8, where in the temperature interval $T \in [1.1, 1.3]$ $z \approx 2$ for TDGL and $z \approx 0.9$ for RSJ; the authors concluded that the TDGL somewhat unexpectedly describes the experiments on Josephson junction arrays by Shaw *et al.*²⁴ better than the RSJ model. The conclusion we arrive at is different since we find that for FTBC the equivalence between RSJ and TDGL is restored. The apparent difference in case of PBC appears to be a boundary effect. We believe that the physical situation in Ref. 24 and most other common experimental situations are in fact better described by the FTBC. Of course, for large enough system sizes, intensive physical quantities do not depend on the explicit choice of boundary condition. But the point here is that, because the relaxation of the zero- k mode is described by a relaxation time τ_G which diverges for infinite systems, the exponent z , which describes how this divergence is approached, appears to be sensitive to the choice of boundary condition.

We also note that for $T = 0.90$ we find $z \approx 1.6$ in case of RSJ with PBC. This suggests that z for PBC approaches a value less than 2 as the KT transition is approached from below, although the numerical accuracy may be insufficient to make a firm conclusion.

B. Dynamics for the Fluctuating Twist Boundary Conditions

In case of FTBC the static dielectric function function $1/\tilde{\epsilon}(\mathbf{k}, 0)$ is identically zero for $\mathbf{k} = 0$, whereas $\lim_{\mathbf{k} \rightarrow 0} 1/\tilde{\epsilon}(\mathbf{k}, 0) \neq 0$ below the KT transition.¹⁶ In

Ref. 10 it was shown that for the Coulomb gas model with Langevin dynamics the function $1/\hat{\epsilon}(\mathbf{k}, \omega)$ for small \mathbf{k} is to good approximation given by the MP form. Since, as explained above in Sec. III, PBC for the vortices (as in Ref. 10) corresponds to FTBC for the XY model we also expect to find the MP form for small k in the present case. This is illustrated in Fig. 5 which shows the real and imaginary parts of $1/\hat{\epsilon}(\mathbf{k}, \omega)$ for $\mathbf{k} = (0, 2\pi/L)$ with $L = 64$ for the XY model with RSJ dynamics. The full drawn and broken curves represent the MP form just as in Fig. 2 and the dotted line shows that the peak ratio is close to $2/\pi$. Figure 6 demonstrates that the imaginary part depends very little on the k value whereas the real part increases with decreasing k for fixed frequency. This behavior has also been found for the Coulomb gas model with Langevin dynamics (compare Figs. 11 and 12 in Ref. 10). Figure 7 shows how the relaxation time τ_G of $\hat{G}(\mathbf{k}, t)$ depends on k : $\hat{G} \propto (e^{-t/\tau_G})/t$ for large t and τ_G diverges as k is decreased. In Ref. 10 it was found that $\tau_G \propto k^{-2}$ for the Coulomb gas model with Langevin dynamics. Our present convergence is not good enough for establishing this result, but Fig. 7(b) suggests that such a behavior is also consistent with the present simulations of the XY model with RSJ dynamics.

Next we turn to the diverging relaxation time τ and the dynamical critical exponent z for the case of FTBC. We will use the fact that in the low-temperature phase the resistance R of a finite system is proportional to $1/\tau$.²⁵ This follows because of the Nyquist formula:²⁶

$$R = \frac{1}{2k_B T} \int_{-\infty}^{\infty} dt \langle V(t) V(0) \rangle. \quad (40)$$

which relates the resistance to the voltage fluctuations over the sample and the fact that $V \propto \frac{d}{dt} \Delta\phi$ where $\Delta\phi$ is the phase difference over the sample. Since $\Delta\phi$ is dimensionless it follows that R scales like $1/\tau$ where τ is the relevant characteristic time.²⁵ In the low-temperature phase R vanishes in the limit of large system sizes since τ diverges. Consequently the finite-size scaling $R \propto 1/\tau \propto L^{-z}$ defines the value of the dynamical critical exponent z in the low-temperature phase. For the XY model with FTBC the phase difference over the sample in one direction (let us choose the x -direction) is given by $\Delta\phi = L\Delta_x$. It follows that R can be expressed as

$$R = \frac{L^2}{2T} \frac{1}{\Theta} \langle [\Delta_x(\Theta) - \Delta_x(0)]^2 \rangle, \quad (41)$$

where T is in units of J/k_B , $\Delta_x(t)$ is the twist variable in the x -direction at time t , and R is in units of the shunt resistance r of a single Josephson junction for the RSJ model and $\Gamma J/2eic$ for TDGL model, respectively. Since Eqs. (40) and (41) are identical in the limit of large Θ , i.e., for $\Theta \gg \tau$,²⁶ we for practical reasons use Eq. (41) in the present simulations (we have used $\Theta = 16000$ and $\Theta \gg \tau$). Figure 8(a) shows the results for the XY model with RSJ dynamics for $T = 0.90, 0.85$ and 0.80 . The data

are plotted as $\log R$ against $\log L$ and to good approximation fall on a straight line, whose slope gives an estimate of the critical exponent z , and we obtain $z = 2.0, 2.7$, and 3.3 , respectively. Figure 8(b) shows the same features for the XY model with TDGL dynamics at the same three temperatures $T = 0.90, 0.85$, and 0.80 and the estimated values of $z \approx 2.1, 2.8$, and 3.3 are close to the ones obtained for the RSJ dynamics.

Thus for the FTBC we find the same z below the KT transition for RSJ and TDGL dynamics, which is in contrast to the PBC case where we found different values of z for each dynamics (compare the discussion of Fig. 4 in Sec. IV). Furthermore for FTBC we find that z apparently approaches 2 when the KT transition is approached from below ($T = 0.90$ is very close to the KT transition temperature) for both dynamics; This did not seem to be true for the RSJ dynamics with PBC ($z \approx 1.6$ at $T = 0.90$). Our conclusion is that the dynamical critical exponent z is a boundary sensitive quantity. We also note that the FTBC is adequate for describing an open system with voltage fluctuation across the system and that consequently the z values obtained for this case describe the most usual physical situation.

It is in fact possible to estimate the characteristic time τ very directly since the variable Δ_x changes by the amount $2\pi/L$ when a vortex moves across the system in the y -direction, as discussed in Sec. III. Every such event consequently is signaled by a 2π -step in the time series of the variable $L\Delta_x$. Figure 9 illustrates this for the RSJ dynamics at $T = 0.85$ for various system sizes. As seen in the figure the 2π -jumps are very well observable. The characteristic time scale τ of these 2π -jumps is easily estimated as the average time between the jumps and we expect that $\tau \sim L^z$ with the same dynamical critical exponent z as in $R \sim L^{-z}$. Figure 10(a) shows τ plotted against the system size L in a log-log plot for the RSJ dynamics for three different temperatures (in practice we use a coarse graining of 100 time units in our estimate of the average time between the 2π -jumps). The full drawn straight lines in Fig. 10(a) have the slopes given by the z values determined previously from the calculation of R [see Fig. 8(a)]. As seen the two ways of determining z agree very well. Figures 8(b) and 10(b) illustrate the same agreement in case of TDGL dynamics.

Let us now consider what happens when a finite current is applied across the system. The scaling argument by Dorsey¹⁹ makes use of the fact that the current density \mathcal{J} introduces a new length scale $1/\mathcal{J}I$.²⁷ This new length scale replaces the finite size L in the leading L dependence of R , so that

$$V = R(\mathcal{J}^{-1})I \propto \frac{1}{\tau(\mathcal{J}^{-1})} I \propto \mathcal{J}^z I$$

and consequently $V \propto I^{z+1}$ below the KT transition as suggested in Ref. 12. From the finite-size scaling of R and τ we hence obtain the non-linear IV exponent a as $a = z + 1$ where $V \propto I^a$. The values obtained are given in Table I.

There are two predictions for the value of a . One is the scaling prediction described in Sec. II [see Eq. (11)¹²]:

$$a_{\text{scale}} = z + 1 = \frac{1}{\tilde{\epsilon}T^{\text{CG}}} - 1,$$

and the other is the AHNS prediction⁴

$$a_{\text{AHNS}} = \frac{1}{2\tilde{\epsilon}T^{\text{CG}}} + 1.$$

In order to compare these predictions with the values of a obtained in the simulations, we need to estimate $1/\tilde{\epsilon}T^{\text{CG}}$. As described in Sec. II, T^{CG} is given by $T^{\text{CG}} = T/(2\pi J\langle U'' \rangle)$ and $1/\tilde{\epsilon} = \lim_{k \rightarrow 0} 1/\tilde{\epsilon}(k, 0)$. However for FTBC we have

$$\frac{1}{\tilde{\epsilon}} = \lim_{k \rightarrow 0} \frac{1}{\tilde{\epsilon}(k, 0)} > \frac{1}{\tilde{\epsilon}(0, 0)} = 0.$$

So for each size L we estimate $1/\tilde{\epsilon}$ by $1/\tilde{\epsilon}(2\pi/L, 0)$. As mentioned in the beginning of this section we can also include a small correction due to the finite time step Δt in the simulations for each size L by replacing T by an effective temperature $T^{\text{eff}} = \hat{G}(0, 0)/\langle U'' \rangle$. Figure 11 shows the two exponents a_{scale} and a_{AHNS} estimated in this way as a function of L . When comparing with the a values obtained from the finite-size scaling of R , we take an average over the relevant L -interval. These values are shown in Table I. As is apparent from Table I, the values of a determined from the size scaling of R and τ agree very well with a_{scale} both for the RSJ case and the TDGL case. Thus we conclude that $z = \frac{1}{\tilde{\epsilon}T^{\text{CG}}} - 2$. This conclusion has also been reached for the lattice Coulomb gas model with Monte Carlo dynamics.¹¹ Furthermore, by invoking the scaling argument described above, we infer that the IV exponent should be given by $a = a_{\text{scale}} = z + 1 = 1/\tilde{\epsilon}T^{\text{CG}} - 1$.¹²

The model given in Ref. 5 suggests the finite-size scaling $R \propto L^{1-a_{\text{scale}}}$ in agreement with our results.²⁹ However, according to the reasoning in Ref. 5, the scaling argument $L \propto 1/\mathcal{J}$ leading to the non-linear IV -exponent $a = a_{\text{scale}}$ should break down for small enough currents and in this limit one should instead recover $a = a_{\text{AHNS}}$.

In the next section we investigate the non-linear IV characteristics more directly by imposing an external current.

V. NON-LINEAR IV CHARACTERISTICS

In order to obtain the IV characteristics for the 2D XY model with RSJ dynamics we use FTBC and Eqs. (33) – (35). Figure 12 shows the data obtained from lattice sizes $L = 4$ to 64, where $v = V/L$ is plotted against $i_d = I_d/L$ in a log-log plot. As seen from the figure the data are size-dependent but for $L = 64$ the data appear to be reasonably size converged except for the smallest currents. The data in the figure are for $T = 0.80$ and the straight

line is a least-square fit to the $L = 64$ data in the current interval $0.03 \leq i_d \leq 0.15$ and gives $a \approx 4.7$, which is in reasonable agreement with $a_{\text{scale}} = 1/\tilde{\epsilon}T^{\text{CG}} - 1 \approx 4.5$. In the following we will investigate the sensitivity of this apparent agreement to finite size, finite current and boundary conditions.

One finite-current effect is that the exponent a refers to a constant Coulomb gas temperature $T^{\text{CG}} = T/[2\pi J\langle U'' \rangle]$. Since a finite current changes the value of $\langle U'' \rangle$,¹² fixed temperature ($T = \text{const.}$) is not entirely equivalent to fixed Coulomb gas temperature ($T^{\text{CG}} = \text{const.}$). In order to convert the data to fixed Coulomb gas temperature we have calculated v and T^{CG} for $T = 0.79$ and 0.80 for fixed external currents, and then by interpolation estimated the voltage value corresponding to a fixed T^{CG} . The resulting data for a fixed Coulomb gas temperature ($T^{\text{CG}} \approx 0.17$) are shown in the inset of Fig. 12. The broken line in the inset is a fit to the data and gives $a \approx 4.5$. Thus this correction leads to a somewhat smaller value of a .

All previous estimates for the non-linear IV exponent for the RSJ model have been obtained for $L = 64$ or smaller sizes.^{9,12,23} The next question we address is how much the possible remaining size effects could alter the results inferred for $L = 64$. Figure 13 shows voltage v versus the system size L at the external current $i_d = 0.1$ and $T = 0.8$ for three different cases. The open squares at the top correspond to the usual uniform current injection method used in Ref. 23. The filled circles correspond to our FTBC boundary condition and finally the open triangles at the bottom correspond to the busbar boundary condition used in Ref. 9.²⁸ It is clear from the figure that $L = \infty$ -result cannot be estimated by the $L = 64$ for $i_d = 0.1$. For smaller i_d the situation quickly gets even worse. Thus this unexpected strong size-dependency clearly makes all earlier results obtained for a from IV simulations somewhat questionable.^{9,12,23}

As seen in Fig. 13 the uniform current injection appears to approach the $L = \infty$ -value from above whereas the FTBC and the busbar condition appear to approach the $L = \infty$ -value from below. We have found this to be generally true. From this we conclude that $L = 256$ is enough to estimate the $L = \infty$ -limit for $i_d > 0.1$, since the data for FTBC and uniform current injection are closely the same in this case. The value of a obtained in this converged current region is about $a \approx 4.1$, which is somewhat smaller than $a \approx 4.3$ obtained from the finite-size scaling of R in the previous section.

In order to get some further insight, we note that the present simulation gives the resistance $R = v/i_d$ as a function of i_d , as discussed in the previous section, for small enough current densities \mathcal{J} , $1/\mathcal{J}$ should corresponds to a finite L . Consequently $R(c/i_d)$, where c is a constant, obtained in the present simulations should be equivalent to $R(L)$ obtained in the previous section: For an appropriate choice of the constant c the data for these two simulations should fall on a single curve. Figure 14 illustrates this equivalence, the filled circles are the data

for $R(L)$ and the open squares are the IV data obtained from FTBC with $L = 256$. The open circles are the averages between the $L = 256$ result for FTBC and uniform current injection. When the open circles and squares overlap, the $L = \infty$ -limit has been reached. As seen from the figure the two data sets for R to a good approximation fall on a single curve. For large currents R approaches the junction resistance $r = 1$ and for small currents $R \propto (i_d)^{a-1}$. The full drawn curve ($R = e^{(a-1)K_0(bi_d)}$ where K_0 is a modified Bessel function) interpolates between these two limits [$K_0(x) \sim -\ln x$ for small x and $K_0(0) = 0$]. Since the converged IV data are higher up on the curve one expects an apparent smaller a than for the $R(L)$ data which are lower down on the curve. Our conclusion is that the results from the IV simulations and the $R(L)$ simulations are consistent with each other and with the scaling assumption.

Scaling Collapse

It is in fact possible to demonstrate the validity of the scaling assumption in a more general way: At fixed temperature R is only a function of L and \mathcal{J} . From the fact that $R \sim 1/L^z$ at $\mathcal{J} = 0$ and that the combination $\mathcal{J}L$ is dimensionless, one expects that

$$R = \left[\frac{f(\mathcal{J}L)}{L} \right]^z, \quad (42)$$

where $f(x)$ is a dimensionless scaling function. The scaling function $f(x)$ must have the limits $f(0) = \text{const.}$ since $R \sim 1/L^z$ for $\mathcal{J} = 0$, and $f(x) \propto x$ for large x . The latter follows because the $L \rightarrow \infty$ -limit has to give a non-vanishing finite R . This means that the combination

$$LR^{1/z} = f(\mathcal{J}L) \quad (43)$$

is only a function of $\mathcal{J}L$. In Fig. 15 we have plotted all our simulation data for $i_d \leq 0.6$ as $LR^{1/z}$ against $i_d L$, i.e., the data shown in Fig. 12 together with data for $L = 128$ and 256 . Using z as an adjustable parameter, we find that all the data collapse onto a single scaling curve for $z \approx 3.3$. We emphasize that this scaling collapse involves only *one* free parameter, z . One also notes that the best value for the collapse (obtained by a least-square method) is closely the same ($z \approx 3.3$ at $T = 0.80$) as was found in the absence of external currents shown in Fig. 8(a). Furthermore this zero- i_d data collapse onto a single value for $z \approx 3.3$ when plotted as $LR^{1/z}$ and this constant value is given by the broken horizontal line in Fig. 15. Thus the data collapse shown in Fig. 15 clearly demonstrates that the scaling assumption is valid for all the data we have obtained. Since the scaling assumption gives $a = a_{\text{scale}} = z + 1 = 1/\epsilon T^{\text{CG}} - 1$, our conclusion is that a_{scale} is indeed the correct IV exponent over a broad parameter range.

The model discussed in Ref. 5 suggests that for small enough i_d the scaling assumption should break down.

Thus for such small currents the data for large enough L should fall above the scaling curve in Fig. 15. There is no sign of any such deviation in our data. However, this does not preclude the possibility that such a deviation could in principle occur for larger sizes and smaller currents than we have been able to investigate.

It is also interesting to note that the scaling function $f(x)$ is intimately connected to the finite-size dependence of the voltage for FTBC. [See, for example, Fig. 13 for $T = 0.8$ and $i_d = 0.1$ (filled circles).] According to Eq. (42) we have

$$v = i_d^{z+1} \left[\frac{f(Li_d)}{Li_d} \right]^z. \quad (44)$$

The full drawn curve in Fig. 16 gives v as a function of L using Eq. (44) for $i_d = 0.1$ where the scaling function $f(x)$ has been obtained by a data smoothing of the data in Fig. 15. The filled circles is a replot of the finite-size dependence given as filled circles in Fig. 13. As is apparent from Fig. 16, the particular shape of the finite-size dependence is a direct reflection of the scaling function $f(x)$.

VI. SUMMARY AND COMPARISONS

The first main result of the present investigation is that the 2D XY model with RSJ dynamics is well described by the MP form for the dynamical response. This appears to be generic for 2D vortex fluctuations since the same form has been found for the XY model with TDGL dynamics,⁷ the 2D Coulomb gas with Langevin dynamics¹⁰ as well as in experiments.^{7,13,14} However, since the 2D XY model with RSJ dynamics is generally accepted as a valid model for a 2D Josephson junction array, the present investigation ties the MP form found in the present and previous simulations closer to the MP form found in experiments.^{7,13}

In one respect we found a difference between the RSJ and the TDGL dynamics. This was the divergence of the relaxation time below the KT transition as a function of the system size for periodic boundary conditions. For example at $T = 0.85$ we found $z \approx 1.6$ in case of RSJ and $z \approx 2$ in case of TDGL. We suggested that this difference might be related to the difference between the TDGL and the RSJ dynamics found in Ref. 8. Next we discovered that this difference was explicitly dependent on the boundary condition used. Thus we found that for the fluctuating twist boundary condition FTBC (which corresponds to PBC for the vortices) the difference in z between the RSJ and the TDGL dynamics disappears. We argued that the FTBC is the appropriate boundary condition for most physical situations. Our conclusion is hence that with the boundary condition which describes the most common physical situations there is no qualitative difference between vortex related properties obtained from RSJ and TDGL dynamics.

Using the FTBC, we could calculate the resistance R in the absence of external currents as a function of the system size L and determine the critical dynamical exponent z below the KT transition. This exponent was found to be the same for RSJ and TDGL dynamics and to support the scaling prediction $z = 1/\tilde{\epsilon}T^{\text{CG}} - 2$ in agreement with what was found in Ref. 11 for the 2D lattice Coulomb gas with Monte Carlo dynamics. We also explicitly showed that the exponent z determined from the finite-size scaling of R is related directly to a diverging relaxation time. Thus our conclusion is that z is larger than 2 below the KT transition. This result is in agreement with the model discussed in Ref. 5.²⁹ Using a scaling argument,¹⁹ we related the finite-size scaling of R to the non-linear IV characteristics by noting that the current density \mathcal{J} plays the role of $1/L$ leading to $V \propto I^a$ with $a = z + 1$. Consequently, provided the scaling argument is valid, our simulations support the prediction $a = 1/\tilde{\epsilon}T^{\text{CG}} - 1$.¹²

We also calculated the IV exponent a directly from the voltage V as a function of current I . Here we found that the results were strongly size-dependent. This large size-dependence we found for standard current injection boundary, FTBC and the “busbar” boundary condition introduced in Ref. 9. For our largest lattice sizes 256×256 a size-converged result could only be estimated for currents which seemed to be outside the true scaling regime $V \propto I^a$. However, by using the relation $L \propto 1/\mathcal{J}$ valid for small enough \mathcal{J} we showed that the data for the resistance simulation $R(L)$ and the IV simulations $R(c/\mathcal{J})$ can be made to fall on a single curve for an appropriate choice of the constant c . This agreement suggests that our IV simulations and our $R(L)$ simulations are consistent with each other and with the scaling assumption. We concluded that it is difficult to obtain the non-linear IV exponent a directly from the $V(I)$ data in case of the 2D XY model with RSJ dynamics. This is because resistance ratios $R(I)/r < 10^{-3}$ (r is the junction resistance) seem to be needed. This in turn implies such small cur-

rents that lattice sizes considerably larger than 256×256 are required to avoid the finite-size effects. However, in case of the 2D Coulomb gas with Langevin dynamics¹⁰ it has been possible to converge the simulations closer to where the true scaling $V \propto I^a$ appears to be valid and in these cases the scaling exponent $a = 1/\tilde{\epsilon}T^{\text{CG}} - 1$ was deduced from the $V(I)$ data.

Finally we showed that all our IV data and our $R(L)$ data for a fixed temperature collapse onto a single scaling curve $f(x = Li_d)$. This data collapse demonstrates that the scaling argument is indeed valid over a broad parameter range and thus confirms that the non-linear IV exponent is given by $a_{\text{scale}} = 1/\tilde{\epsilon}T^{\text{CG}} - 1$ over the parameter range covered by our data. This does not preclude the possibility that, for smaller currents and larger sizes than we have been able to converge, there might be a deviation from the scaling curve given in Fig. 15 as suggested by the model in Ref. 5. However, there is no sign of any deviation from the scaling curve in our data for the RSJ model.

In short, the present simulations of the 2D XY model with RSJ dynamics confirm the picture that 2D vortex fluctuations has an anomalous kind of dynamics. The characteristic features of this dynamics are presumably linked to the logarithmic vortex interaction. However, a firmer theoretical understanding of the characteristic features, which have been encountered in numerous simulations as well as in experiments, is still lacking and is a challenge for future research.

ACKNOWLEDGMENTS

One of the authors (B.J.K.) wishes to acknowledge the financial support of Korea Research Foundation for the program year 1997. The research was supported by the Swedish Natural Research Council through contracts FU 04040-332 and EG 10376-310.

APPENDIX: LINEAR RESPONSE

A total current $i_x(\mathbf{r}, t)$ which varies slowly in time compared to the thermal fluctuations gives rise to an average non-vanishing phase difference $q(\mathbf{r}, t) = \langle \nabla_x \theta(\mathbf{r}, t) \rangle$. Thus Eqs. (13) and (14) together with the chain rule gives

$$\dot{P}(\mathbf{r} - \mathbf{r}', t - t') = -J \int d^2 r'' dt'' \left. \frac{\partial \langle U'[\nabla_x \theta(\mathbf{r}, t)] \rangle}{\partial q(\mathbf{r}'', t'')} \right|_0 \cdot \left. \frac{\partial \langle \nabla_x \theta(\mathbf{r}'', t'') \rangle}{\partial i_x(\mathbf{r}', t')} \right|_0 + \delta(\mathbf{r} - \mathbf{r}') \delta(t - t'), \quad (\text{A1})$$

where $|_0$ denote that the resulting averages should be the equilibrium ones. Let us introduce the notation

$$Q(\mathbf{r} - \mathbf{r}'', t - t'') = J \left. \frac{\partial \langle U'[\nabla_x \theta(\mathbf{r}, t)] \rangle}{\partial q(\mathbf{r}'', t'')} \right|_0$$

then the Fourier transform of Eq. (A1) is just

$$i\omega \hat{P}(\mathbf{k}, \omega) = -\hat{Q}(\mathbf{k}, \omega) \hat{P}(\mathbf{k}, \omega) + 1 \quad (\text{A2})$$

so that

$$\hat{P}(\mathbf{k}, \omega) = \frac{1}{i\omega + \hat{Q}(\mathbf{k}, \omega)}.$$

We note that

$$\begin{aligned} Q(\mathbf{r} - \mathbf{r}', t - t') &= J \left. \frac{\partial \langle U'[\nabla_x \theta(\mathbf{r}, t)] \rangle}{\partial q(\mathbf{r}', t')} \right|_0 \\ &= J \langle U''[\nabla \theta(\mathbf{r}, t)] \rangle \delta(\mathbf{r} - \mathbf{r}') \delta(t - t') + J \left. \frac{\partial \langle U'[\nabla_x \theta(\mathbf{r}, t)] \rangle}{\partial q(\mathbf{r}', t')} \right|_0. \end{aligned}$$

Here the last term is for $t \neq t'$ and $r \neq r'$ so that the disturbance $q(\mathbf{r}', t') = \langle \nabla_x \theta(\mathbf{r}', t') \rangle$ couples linearly to $JU'[\nabla_x \theta(\mathbf{r}', t')]$ in the XY -Hamiltonian. Consequently, the corresponding correlation function is

$$-J^2 \langle U'[\nabla_x \theta(\mathbf{r}, t)] U'[\nabla_x \theta(\mathbf{r}', t')] \rangle$$

and by the fluctuation-dissipation theorem we have

$$Q(\mathbf{r}, t) = \frac{J^2}{T} \frac{\partial}{\partial t} \langle U'[\nabla_x \theta(\mathbf{r}, t)] U'[\nabla_x \theta(0, 0)] \rangle + J \langle U''[\nabla_x \theta(0, 0)] \rangle \delta(\mathbf{r}) \delta(t)$$

for $t \geq 0$ and 0 otherwise. Next we note that a space Fourier transform of the correlation function $J^2 \langle U'[\nabla_x \theta(\mathbf{r}, t)] U'[\nabla_x \theta(\mathbf{r}', t')] \rangle$ gives the correlation function $\hat{G}(\mathbf{k}, t)$ defined in connection with Eq. (3) so that

$$\begin{aligned} \hat{Q}(\mathbf{k}, \omega) &= \int_0^\infty dt e^{-i\omega t} \hat{Q}(\mathbf{k}, t) = \rho_0 + \frac{1}{T} \int_0^\infty dt e^{-i\omega t} \frac{\partial}{\partial t} \hat{G}(\mathbf{k}, t) \\ &= \rho_0 - \frac{1}{T} \hat{G}(\mathbf{k}, 0) - \frac{1}{T} \int_0^\infty dt e^{-i\omega t} \hat{G}(\mathbf{k}, t) = \frac{\rho_0}{\hat{\epsilon}(\mathbf{k}, \omega)}, \end{aligned} \quad (\text{A3})$$

where $\rho_0 = J \langle U'' \rangle$ and the result is obtained by partial integration and comparison with Eqs. (4)–(6).

¹ J.M. Kosterlitz and D.J. Thouless, *J. Phys. C* **5**, L124 (1972); *J. Phys. C* **6**, 1181 (1973); V.L. Berezinskii, *Zh. Eksp. Teor. Fiz.* **61**, 1144 (1972) [*Sov. Phys. JETP* **34**, 610 (1972)].

² For a general review see, e.g., P. Minnhagen, *Rev. of Mod. Phys.* **59**, 1001 (1987).

³ For a recent reviews see, e.g., K.H. Fischer, *Superconductivity Review* **1**, 153 (1995); P. Minnhagen in “Enrico Fermi” Course CXXXVI: *Models and Phenomenology for Conventional and High-Temperature Superconductors*.

⁴ V. Ambegaokar, B.I. Halperin, D.R. Nelson, and E.D. Siggia, *Phys. Rev. Lett.* **40**, 783 (1978); *Phys. Rev. B* **21**, 1806 (1980); V. Ambegaokar and S. Teitel, *ibid.* **19**, 1667 (1979).

⁵ D. Bormann, *Phys. Rev. Lett.* **78**, 4324 (1997).

⁶ M. Capezzali, H. Beck, and S.R. Shenoy, *Phys. Rev. Lett.* **78**, 523 (1997).

⁷ A. Jonsson and P. Minnhagen, *Phys. Rev. B* **55**, 9035 (1997); *Physica C* **277**, 161 (1997).

⁸ P.H.E. Tiesinga, T.J. Hagenraars, J.E. van Himbergen, and J. V. José, *Phys. Rev. Lett.* **78**, 519 (1997).

⁹ M.V. Simkin and J.M. Kosterlitz, *Phys. Rev. B* **55**, 11 646 (1997).

¹⁰ K. Holmlund and P. Minnhagen, *Phys. Rev. B* **54**, 523 (1996); *Physica C* **292**, 255 (1997).

¹¹ H. Weber, M. Wallin, and H.J. Jensen, *Phys. Rev. B* **53**, 8566 (1996).

¹² P. Minnhagen, O. Westman, A. Jonsson, and P. Olsson, *Phys. Rev. Lett.* **74**, 3672 (1995).

¹³ R. Théron, J.-B. Simond, Ch. Leemann, H. Beck, P. Martinoli, and P. Minnhagen, *Phys. Rev. Lett.* **71**, 1246 (1993).

¹⁴ C.T. Rogers, K.E. Myers, J.N. Eckstein, and I. Bozovic, *Phys. Rev. Lett.* **69**, 160 (1992).

¹⁵ E. Domany, M. Schick, and R.H. Swendsen, *Phys. Rev. Lett.* **52**, 1535 (1984).

¹⁶ P. Olsson, *Phys. Rev. B* **46**, 14 598 (1992); *ibid.* **52**, 4511 (1995); *ibid.* **52**, 4526 (1995); Ph. D. thesis, Umeå University, 1992.

¹⁷ D.R. Nelson and J.M. Kosterlitz, *Phys. Rev. Lett.* **39**, 1201 (1977).

¹⁸ P. Minnhagen and G.G. Warren, *Phys. Rev. B* **24**, 2526 (1981).

¹⁹ A.T. Dorsey, *Phys. Rev. B* **43**, 7575 (1991).

²⁰ B.I. Halperin and D.R. Nelson, *J. Low Temp. Phys.* **36**, 599 (1979).

²¹ J. Houlrik, A. Jonsson, and P. Minnhagen, *Phys. Rev. B* **50**, 3953 (1994).

²² H. Risken, *The Fokker-Planck Equation* (Springer-Verlag, Berlin, 1984).

²³ K.K. Mon and S. Teitel, Phys. Rev. Lett. **62**, 673 (1989).
²⁴ T.J. Shaw, M.J. Ferrari, L.L. Sohn, D.-H. Lee, M. Tin-kham, and J. Clarke, Phys. Rev. Lett. **76**, 2551 (1996).
²⁵ M. Wallin and H. Weber, Phys. Rev. B **51**, 6163 (1995).
²⁶ F. Reif, *Fundamentals of Statistical and Thermal Physics* (McGraw Hill, 1965).
²⁷ M.P.A. Fisher, Phys. Rev. Lett. **62**, 1415 (1989); D.S. Fisher, M.P.A. Fisher, and D.A. Huse, Phys. Rev. B **43**, 130 (1991).
²⁸ For convenience we used an approximate version of the busbar idea by using uniform current injection but with the coupling between the junctions at the boundary 10 times larger than the others. We found that this procedure closely reproduce the strict busbar condition.
²⁹ D. Bormann (private communication).

TABLE I. Comparison between the exponent $a \equiv z + 1$ obtained from the $R(L)$ simulations and the predicted values a_{scale} and a_{AHNS} for (a) RSJ and (b) TDGL dynamics. The values of a_{scale} and a_{AHNS} are obtained from the averages over $L = 10, 12$, and 16 (see Fig. 11 for RSJ case). The exponent $a \equiv z + 1$ is obtained from $R(L) \sim L^{-z}$ in Fig. 8 and is found to be consistent with z in $\tau \sim L^z$ in Fig. 10. The numbers in parenthesis represent the statistical errors of the last digits. It is clearly shown that the exponent a measured by direct calculation of resistance from Eq. (41) is much closer to a_{scale} than to a_{AHNS} for both RSJ and TDGL dynamics.

(a) RSJ

T	a_{scale}	a_{AHNS}	a
0.80	4.42(2)	3.71(2)	4.3(1)
0.85	3.80(2)	3.40(2)	3.7(1)
0.90	3.05(2)	3.02(2)	3.0(1)

(b) TDGL

T	a_{scale}	a_{AHNS}	a
0.80	4.55(3)	3.77(2)	4.3(1)
0.85	3.85(2)	3.43(2)	3.8(1)
0.90	3.12(2)	3.06(1)	3.1(1)

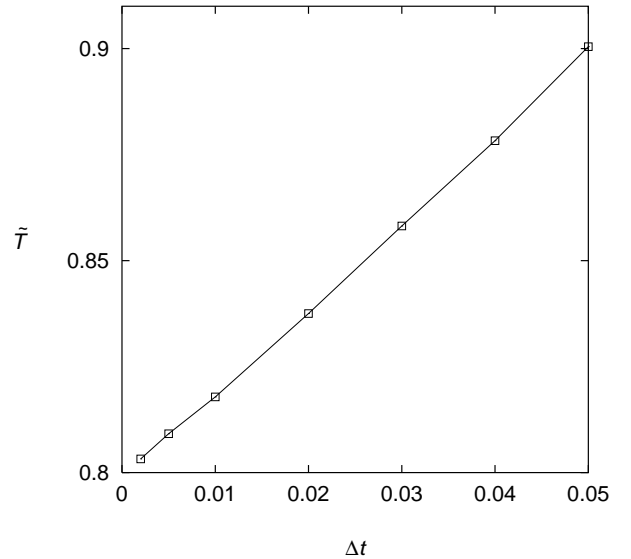


FIG. 1. The temperature \tilde{T} as a function of the integration time step Δt at $T = 0.8$ for TDGL dynamics [see Eq. (37)]. \tilde{T} approaches T , as Δt approaches zero (the full line is a guide to the eye).

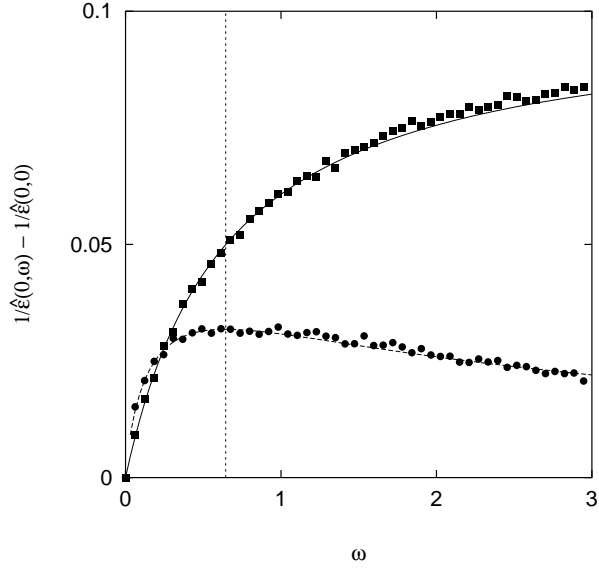


FIG. 2. The dynamical response function $1/\hat{\epsilon}(0, \omega)$ of the 2D XY model with RSJ dynamics at $T = 0.85$ for a 64×64 -lattice with periodic boundary conditions. The filled squares and circles correspond to the real part and the absolute value of the imaginary part of the dynamical response function, respectively. The full curve is obtained by fitting to the real part of the MP form response function in Eq. (8) and the broken curve is the imaginary part Eq. (9) using the same values of the fitting parameters as for the full curve. The vertical broken line corresponds to the ω for which the peak ratio $|\text{Im}[1/\hat{\epsilon}(0, \omega)]|/\text{Re}[1/\hat{\epsilon}(0, \omega) - 1/\hat{\epsilon}(0, 0)]$ is $2/\pi$. At this ω the absolute value of the imaginary part should, according to the MP form, have a maximum.

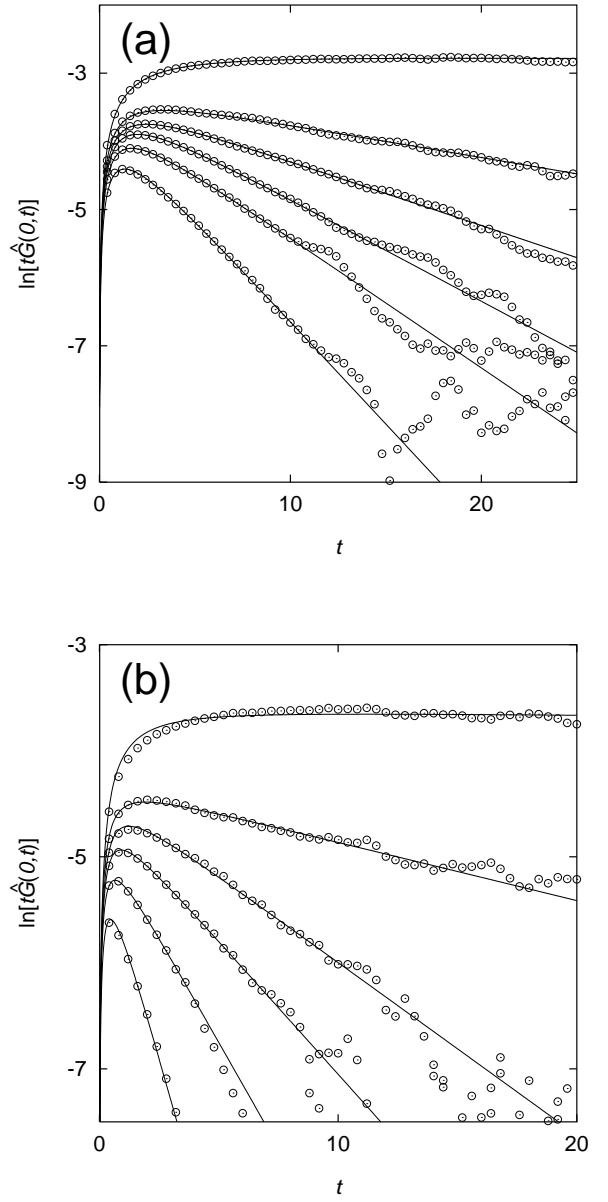


FIG. 3. The time-correlation function $\ln[t\hat{G}(0, t)]$ versus time t at $T = 0.85$ for various system sizes [$L = 6, 8, 10, 12, 16$, and 64 from bottom to top] in case of (a) RSJ and (b) TDGL dynamics. The full curves have been obtained by fitting to the modified-MP (MMP) form Eq. (39). The figure shows that the relaxation time τ_G in the MMP form diverges as the system size is increased and that $\hat{G}(0, t) \propto 1/t$ for large t in the thermodynamic limit.

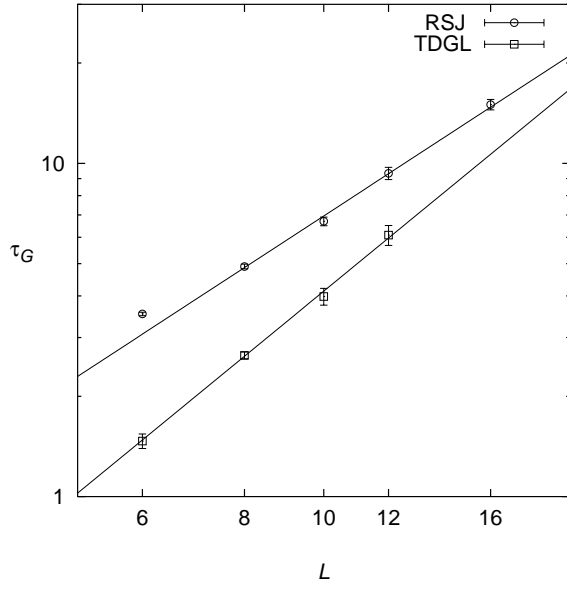


FIG. 4. The relaxation time τ_G for the time-correlation function $\hat{G}(0, t)$ at $T = 0.85$ for RSJ (squares) and TDGL (circles) dynamics. The data points have been obtained from least-square fits to the MMP form \hat{G}^{MMP} given by Eq. (39) as shown in Fig. 3. As the system size L is increased τ_G diverges. However, the exponent z defined by $\tau_G \sim L^z$ appears to have *different* values for the two types of dynamics. The lines are obtained from least-square fits using data points for $L = 8, 10, 12$, and 16 in the RSJ case and $L = 6, 8, 10, 12$ in the TDGL case, giving $z \approx 1.6$ and $z \approx 2.0$ for RSJ and TDGL, respectively.

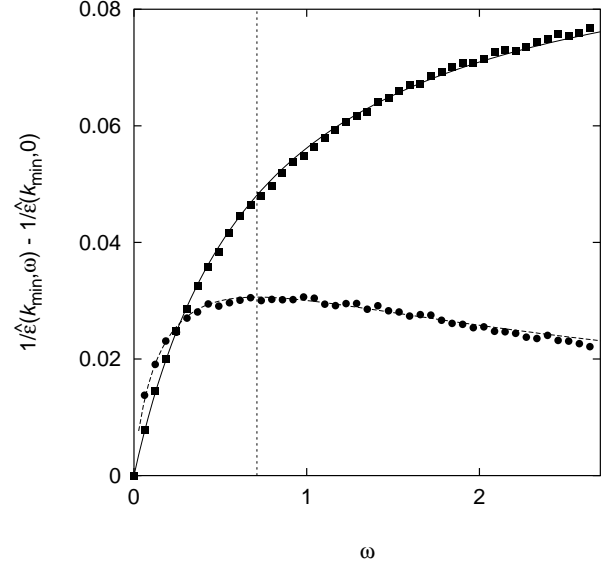


FIG. 5. The dynamical response function $1/\hat{\epsilon}(\mathbf{k}, \omega)$ at $\mathbf{k} = \mathbf{k}_{\min} \equiv (0, 2\pi/L)$ for a $L = 64$ array at $T = 0.85$ for RSJ dynamics with FTBC. The filled squares and circles correspond to the real part and (the absolute value of) the imaginary part of $1/\hat{\epsilon}(\mathbf{k}, \omega)$. The full curve is obtained from a least-square fit to Eq. (8) with two free parameters ω_0 and $\tilde{\epsilon}$ and the broken curve is obtained from Eq. (9) using these parameter values. The vertical broken line is given by the condition that the peak ratio $|\text{Im}[1/\hat{\epsilon}(\mathbf{k}, \omega)]|/\text{Re}[1/\hat{\epsilon}(\mathbf{k}, \omega) - 1/\hat{\epsilon}(\mathbf{k}, 0)] = 2/\pi$ and at this value of ω , the absolute value of the imaginary part should, according to the MP form, have a maximum.

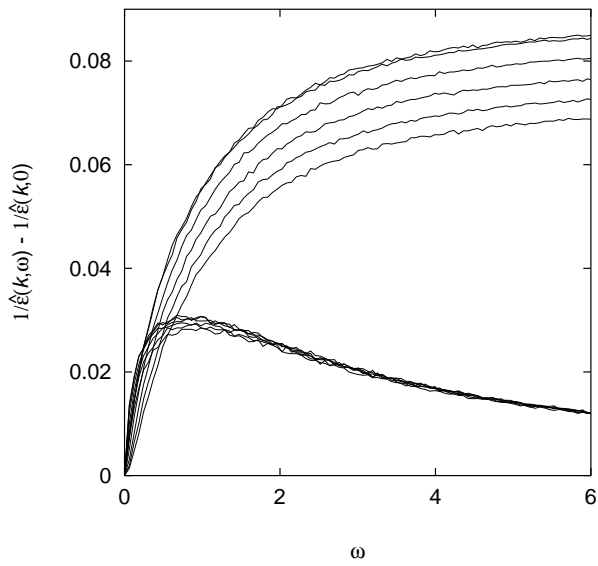


FIG. 6. The dynamical response function $1/\hat{\epsilon}(\mathbf{k}, \omega)$ at finite \mathbf{k} for a $L = 64$ array at $T = 0.85$ for RSJ dynamics with FTBC. The real and imaginary parts are obtained using the wave vectors $\mathbf{k} = (0, k_y = 2\pi n_y/L)$ with $n_y = 1, 2, 4, 6, 8$, and 10 (from top to bottom). The imaginary part depends very little on the value of k in the frequency interval around the maximum, in contrast to the real part which increases with decreasing k .

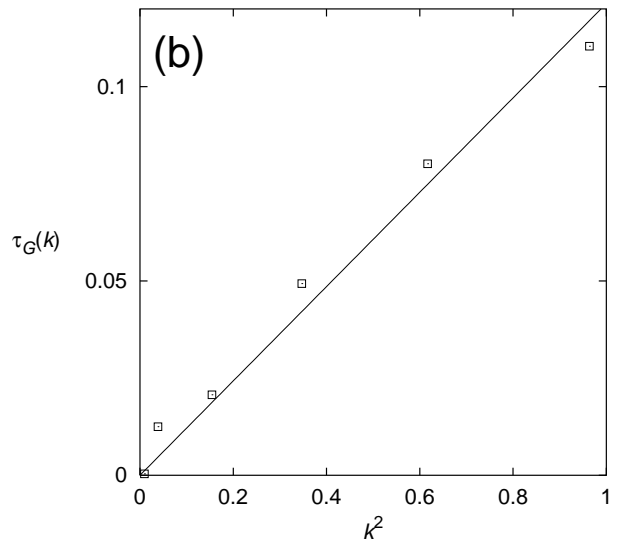
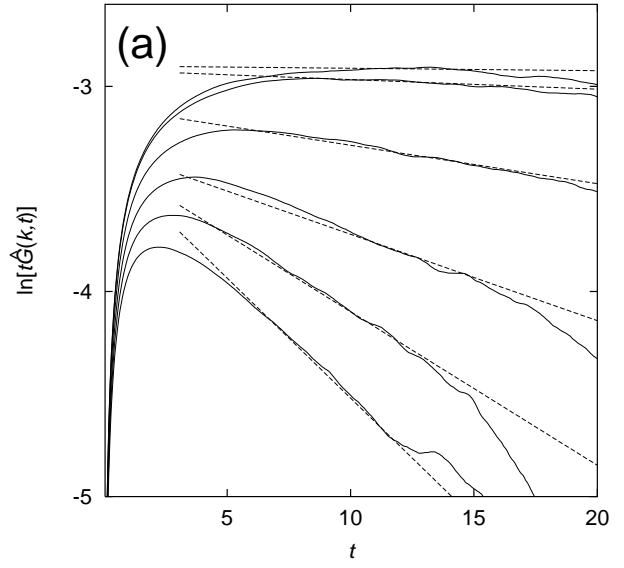


FIG. 7. (a) The time-correlation function $\ln[t\hat{G}(\mathbf{k}, t)]$ versus time t at $T = 0.85$ for RSJ dynamics with FTBC. The wave vectors are $\mathbf{k} = (0, k_y = 2\pi n_y/L)$ with $n_y = 1, 2, 4, 6, 8$, and 10 (from top to bottom) and the array size is $L = 64$. As $\mathbf{k} \rightarrow 0$, $\hat{G}(\mathbf{k}, t)$ approaches $\hat{G}(\mathbf{k}, t) \rightarrow 1/t$ for large values of t . At non-zero value of k , $\hat{G}(k, t)$ exhibits exponential decay $\hat{G}(k, t) \sim \exp[-t/\tau_G(k)]/t$ in the long time limit. The broken lines are plotted with the $\tau_G(k)$ values corresponding to the straight line in (b), where we show $\tau_G(k)$ versus k^2 . In (b), the squares have been obtained from the least-square fit of $\hat{G}(k, t)$ to the exponential decay form, and the full straight line is the result of the least-square fit to $\tau_G(k) \propto k^2$.

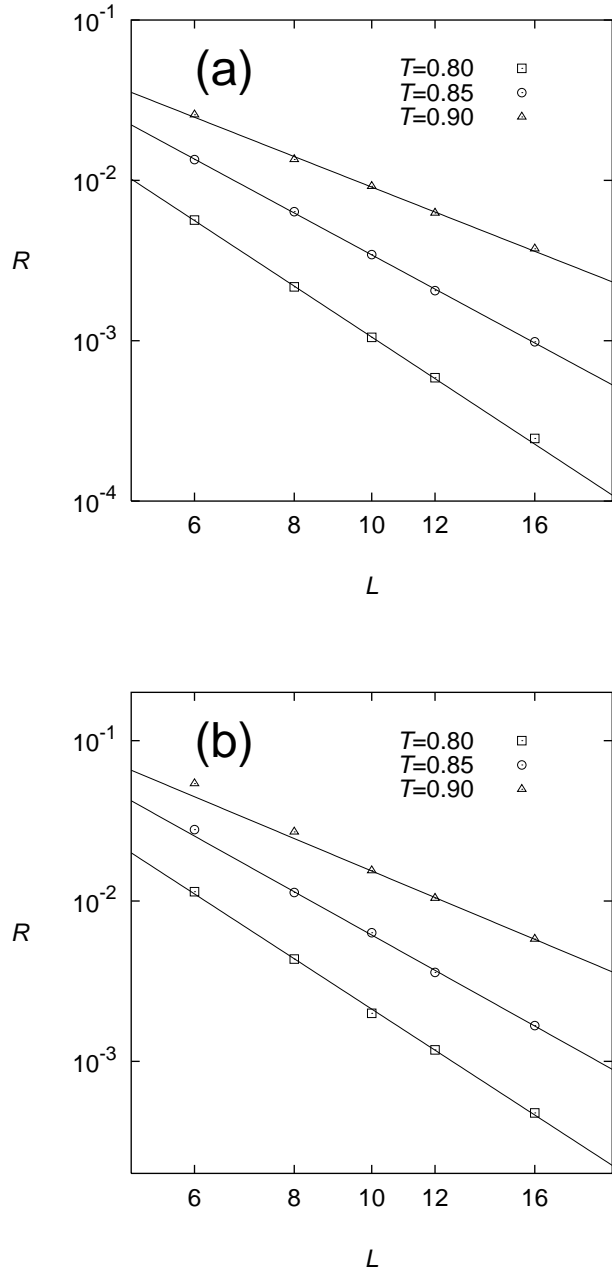


FIG. 8. Resistance R versus system size L for (a) RSJ and (b) TDGL dynamics obtained from Eq. (41). The full lines are obtained by fitting to the scaling form $R \sim L^z$ and from these fits the values of z are determined to be $z = 3.3(1)$, $2.7(1)$, and $2.0(1)$ at $T = 0.80$, 0.85 , and 0.90 for the RSJ case, and $z = 3.3(1)$, $2.8(1)$, and $2.1(1)$ at $T = 0.80$, 0.85 , and 0.90 for TDGL.

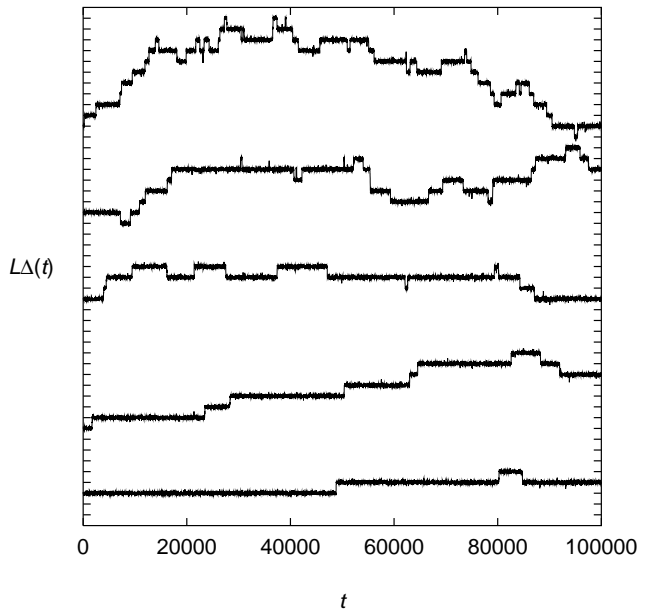


FIG. 9. Time evolution of the variable $L\Delta(t)$ at $T = 0.85$ as a function of time t for RSJ dynamics and system sizes $L = 6, 8, 10, 12$, and 16 (from top to bottom). The curves are shifted in the vertical direction. As seen $L\Delta(t)$ sometimes makes discrete jumps of size 2π (the unit of the vertical axis is 2π). The characteristic time τ in Fig. 10 is related to the average time between the 2π -jumps.

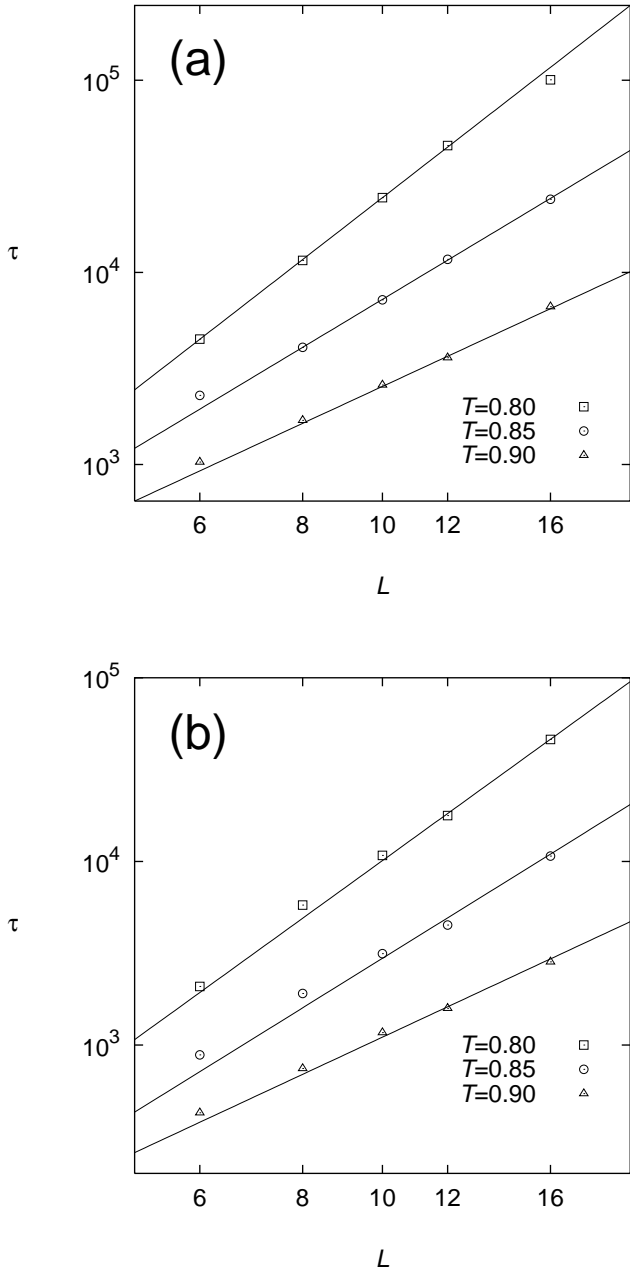


FIG. 10. The relaxation time τ obtained directly from the time scale of the 2π -jumps of $L\Delta(t)$. The obtained values of τ are plotted against the system size L for (a) RSJ and (b) TDGL dynamics. (See Fig. 9.) The full lines represent $\tau \sim L^z$ with the z values taken from Fig. 8. The figure illustrates that z determined from the scaling of the resistance R is indeed associated with a divergent characteristic time.

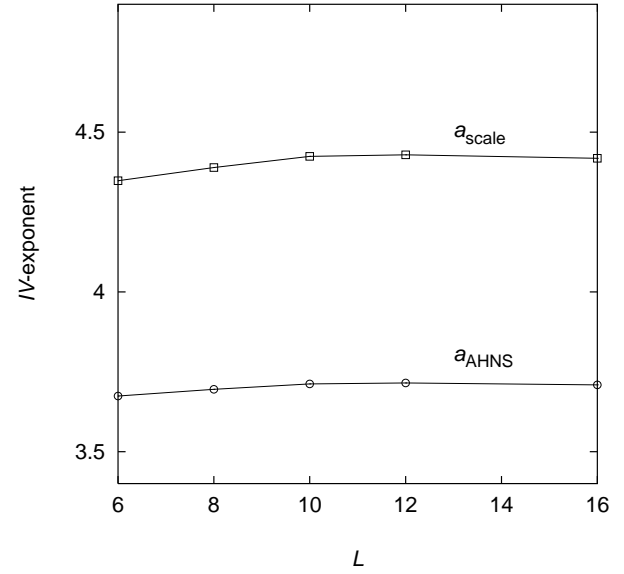


FIG. 11. Predictions of the IV exponent for the RSJ model at $T = 0.8$ as a function of the system size L . The open squares are obtained from $a_{\text{scale}} = 1/\tilde{\epsilon}T_{\text{eff}}^{\text{CG}} - 1$ for FTBC whereas the open circles represent $a_{\text{AHNS}} = 1/2\tilde{\epsilon}T_{\text{eff}}^{\text{CG}} + 1$ for FTBC.

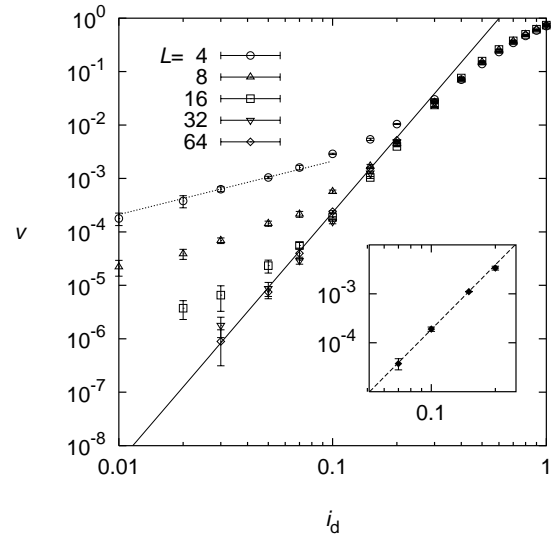


FIG. 12. The current-voltage (IV) characteristics at $T = 0.8$ for the fluctuating twist boundary condition at various system sizes. The full straight line is obtained from the least-square fit in the interval $0.03 \leq i_d \leq 0.15$ for $L = 64$ which gives $a \approx 4.7$. The linear region with IV exponent $a = 1$, seen for the smaller sizes and small currents (the dotted straight line has the slope $a = 1$), disappears as the system size is increased. Inset: IV curve for $L = 64$ at fixed Coulomb gas temperature $T^{\text{CG}} \approx 0.17$, corresponding to $T = 0.80$ with no external currents. The broken line is obtained from the least-square fit in the interval $0.07 \leq i_d \leq 0.15$, giving $a \approx 4.5$.

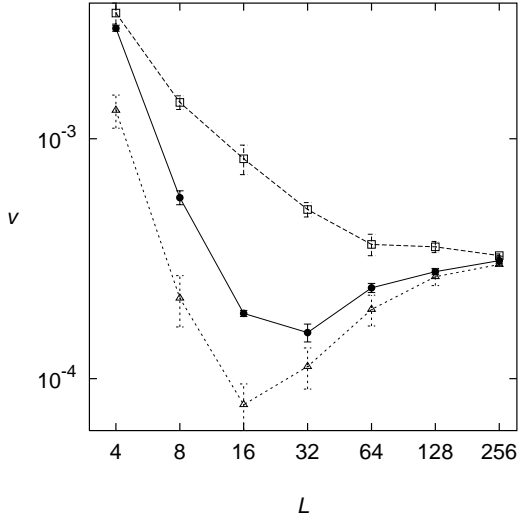


FIG. 13. Voltage v versus system size L at the current $i_d = 0.1$ for $T = 0.8$. The empty squares are for the uniform current injection with periodic boundary conditions in the direction perpendicular to the current. The empty triangles are obtained with the critical current $i_c = 10$ for vertical junctions on the boundaries, which is very similar to the busbar boundary. The filled circles are for FTBC introduced in Sec. III. As the system size is increased, the voltages for all three methods are shown to converge towards the same value in the $L = \infty$ -limit. However, the uniform current injection approaches the $L = \infty$ -limit from above whereas the FTBC and busbar condition approach from below. The lines are guides to the eye.

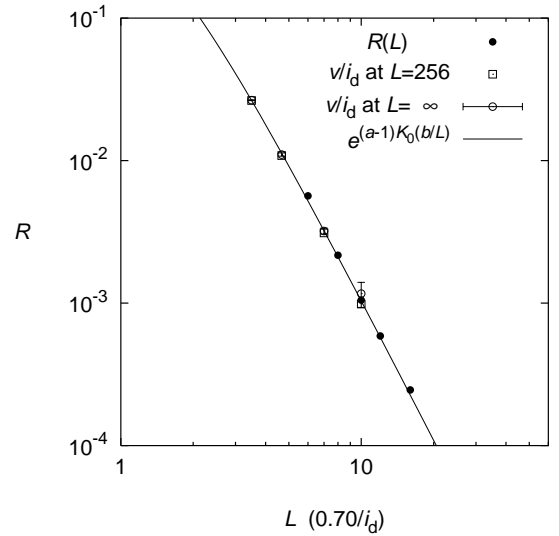


FIG. 14. The resistance $R(c/i_d) = v/i_d$ at $T = 0.80$ (open squares correspond to the $L = 256$ data for FTBC and open circles to the average between the $L = 256$ data for FTBC and the uniform current injection) is compared to the resistances $R(L)$ at $T = 0.80$ [filled circles, the same data as in Fig. 8 (a)]. Choosing the constant $c \approx 0.70$ makes the two data sets collapse onto a single curve. The full drawn curve interpolates between the limits $R = 1$ for large currents and $R \propto (i_d)^{a-1}$ for small currents (the explicit form of the interpolation curve is $e^{(a-1)K_0(b/L)}$ with $a = 4.3$ and $b = 1.42$). The figure suggests that the two ways of calculating R are consistent and that the $R(c/i_d)$ -data are not quite in the asymptotic small-current regime.

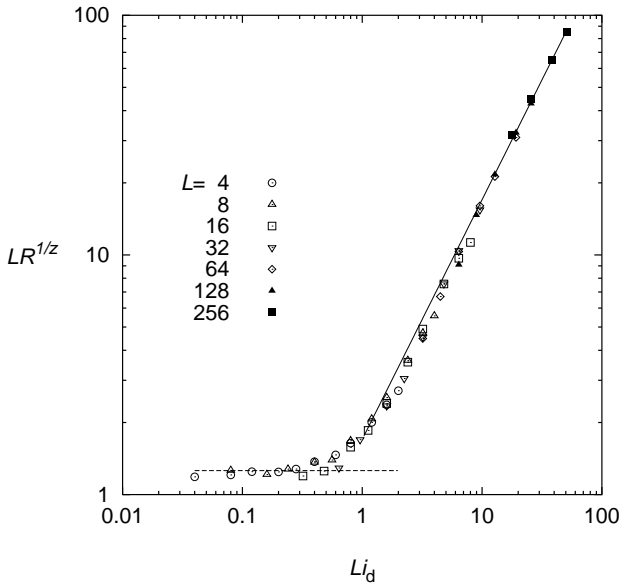


FIG. 15. Demonstration of the validity of the scaling assumption. The IV data for the RSJ model with $T = 0.8$ and $i_d \leq 0.6$ are plotted as $LR^{1/z}$ against Li_d . For $z \approx 3.3$ all the data for the various L and i_d collapse onto a single scaling function $f(x = Li_d)$. The horizontal broken line corresponds to the constant value for $LR(L)^{1/z}$ obtained for $i_d = 0$ for the same value of z [see Fig. 8(a)]. The straight line corresponds to the linear behavior $f(x) \sim x$ for large x .

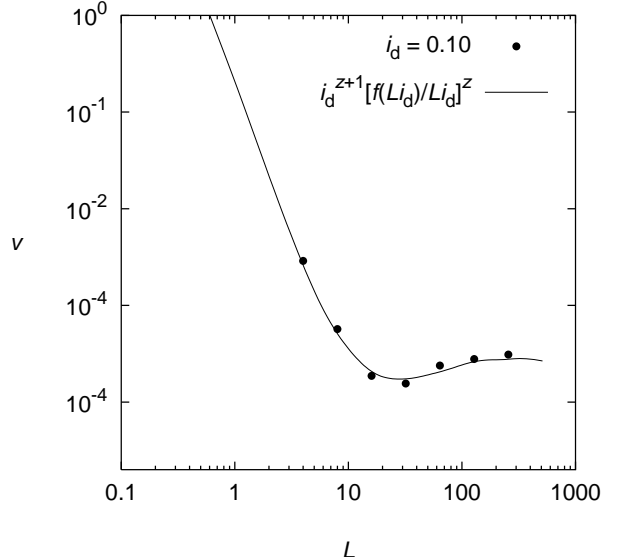


FIG. 16. The relation between the finite-size dependence of the voltage v and the scaling function $f(x = Li_d)$. The full drawn curve is the function $v = i_d^{z+1} [f(x)/x]^z$ where $f(x)$ has been obtained by a data smoothing of the data in Fig. 15. The filled circles are the finite-size data for v at $T = 0.8$, the same data as the filled circles in Fig. 13.